*J. Fluid Mech.* (1996), *vol.* 306, *pp.* 183–221



# One- and two-dimensional travelling wave solutions in gas-fluidized beds

By B. J. GLASSER, I. G. KEVREKIDIS AND S. SUNDARESAN

Department of Chemical Engineering, Princeton University, Princeton, New Jersey 08544, USA

(Received 23 February 1995 and in revised form 10 July 1995)

Making use of numerical continuation techniques as well as bifurcation theory, both one- and two-dimensional travelling wave solutions of the ensemble-averaged equations of motion for gas and particles in fluidized beds have been computed. One-dimensional travelling wave solutions having only vertical structure emerge through a Hopf bifurcation of the uniform state and two-dimensional travelling wave solutions are born out of these one-dimensional waves. Fully developed two-dimensional solutions of high amplitude are reminiscent of bubbles. It is found that the qualitative features of the bifurcation diagram are not affected by changes in model parameters or the closures. An examination of the stability of one-dimensional travelling wave solutions to two-dimensional perturbations suggests that two-dimensional solutions emerge through a mechanism which is similar to the overturning instability analysed by Batchelor & Nitsche (1991).

## 1. Introduction

A uniform suspension of solid particles supported against gravity by an upward flowing fluid, an ideal fluidized bed, is rarely realized in practice. Instead, voidage non-uniformities are observed to move through the bed. In the case of gas-fluidized beds these voidage non-uniformities often take the form of 'bubbles' of almost clear gas. Jackson (1963*a*), Pigford & Baron (1965), Anderson & Jackson (1967, 1968), Garg & Pritchett (1975) and others modelled the fluidized bed using volume-averaged equations of continuity and motion, and analysed the linear stability of the state of uniform fluidization. It was found that the uniform state is always unstable to small disturbances in the absence of a term in the particle-phase momentum equation having the form of a pressure associated with the particle phase.

The existence of voidage waves (in one space dimension) in fluidized beds has been explored previously by Anderson & Jackson (1968, 1969), El-Kaissy & Homsy (1976) and Homsy, El-Kaissy & Didwania (1980). This provided an incentive to understand the structure of the one-dimensional waves in greater detail, taking into consideration the nonlinear effects (Fanucci, Ness & Yen 1979, 1981; Liu 1982, 1983; Needham & Merkin 1983, 1986; Foscolo & Gibilaro 1984, 1987; Ganser & Drew 1990). Fanucci *et al.* (1979) applied the method of characteristics to nonlinear equations describing two-phase flow in a gas-fluidized bed and showed that small disturbances can grow to form a discontinuity (two-phase shock). In a later paper (Fanucci *et al.* 1981) they examined the structure and stability of this shock. It was

shown that two-phase shocks have a limited range of shock propagation speeds. They suggested that the process of breakup of the one-dimensional unstable shocks should be identified with bubble development. Bouillard & Gidaspow (1991) examined the relationship between bubbles and one-dimensional voidage shocks and went on to examine the behaviour of the shocks for different particle sizes. Foscolo & Gibilaro (1984, 1987) performed both linear and nonlinear analyses of the one-dimensional waves and they formulated a hydrodynamic criterion for the onset of bubbling in fluidized beds.

Needham & Merkin (1983, 1986) examined the time evolution of a localized one-dimensional voidage disturbance in an otherwise uniform gas-fluidized bed. It was shown that there is a one-parameter family of quasi-steady periodic states at each flow rate for which the uniform state is unstable. This family of quasi-steady periodic states, parametrized by their propagation velocity, was determined and it was found that the periodic states existed for a limited range of propagation velocities, in agreement with the earlier results of Fanucci *et al.* (1981).

Didwania & Homsy (1982) examined a resonant sideband instability as a means of explaining the instability of a one-dimensional wave in a liquid-fluidized bed. Needham & Merkin (1984) carried out two-dimensional linear calculations and observed the appearance of mushroom-shaped regions of high voidage. Göz (1992) performed a two-dimensional bifurcation analysis of the equations looking at solutions of small amplitude. In particular, instabilities of the uniform state were rigorously characterized and small-amplitude two-dimensional patterns that could develop into bubble-like structures were discussed. Göz (1992, 1993*b*) conjectured that the one-dimensional plane travelling wave might undergo a transversal instability giving rise to a travelling wave with structure in both the vertical and lateral direction. Göz (1995*a*,*b*) went on to show that such an instability can in fact occur. In addition an extensive bifurcation analysis of vertically and obliquely travelling plane waves was carried out by Göz (1993*a*).

Batchelor & Nitsche (1991) examined the stability of a stationary unbounded stratified fluid of variable density. It was found that the fluid is unstable and there is an overturning instability which 'tilts' the layers of stratified fluid. Since a dispersion of small particles in a fluid with non-uniform concentration behaves dynamically like a continuum with non-uniform density in certain circumstances, they suggested that their results might help explain the instability of a voidage wave with horizontal wave front in a fluidized bed. Batchelor (1993) went on to consider the secondary instability of a gas-fluidized bed and found that plane sinusoidal waves with horizontal wave fronts were unstable under practical conditions.

Numerical integration of the volume-averaged equations of motion for gas-fluidized beds has revealed bubble-like structures (Pritchett, Blake & Garg 1978; Gidaspow, Syamlal & Seo 1986; Syamlal & O'Brien 1989; Kuipers, Prins & Van Swaaij 1991; Hernández & Jiménez 1991; Anderson, Sundaresan & Jackson 1995.) Hernández & Jiménez (1991) described the evolution of spatially periodic two-dimensional solutions which result from a secondary instability of the planar vertical travelling wave in gas-fluidized beds.

Anderson *et al.* (1995) integrated the ensemble-averaged equations of motion in two dimensions, assuming spatial periodicity. They found that two-dimensional disturbances in a gas-fluidized bed (200 μm glass beads fluidized by ambient air) developed bubble-like structures for all initial conditions considered. The behaviour of liquid-fluidized beds (1 μm glass beads fluidized by water) was markedly different. When a small two-dimensional disturbance was imposed on a fully developed planar

vertical travelling wave, a bubble-like hole was formed, only to be destroyed shortly afterwards. A small two-dimensional disturbance imposed on an unstable uniform state did not develop a bubble-like structure at any time during the course of their numerical integration. For both initial conditions, the solutions continued to change with time without appearing to settle down into any recognizable pattern. Furthermore, the time-dependent spatial structures observed in these two cases revealed no identifiable similarity.

While the study of Anderson *et al.* (1995) revealed that non-uniform structures in gas- and liquid-fluidized beds evolve differently, the extent of their investigation was limited. Transient integrations of the ensemble-averaged equations of motion were carried out for a small number of initial conditions and model parameters. In the liquid-fluidized bed case integration was not carried out long enough to identify the structure of a fully developed two-dimensional travelling wave. The results of Anderson *et al.* (1995) for the gas-fluidized bed suggest that there are stable two-dimensional solutions to the ensemble-averaged equations of motion. Their results also indicate that these solutions do not change as they move through the bed at constant velocity.

In the present manuscript, a detailed computational analysis of fully developed one- and two-dimensional travelling wave solutions of the ensemble-averaged equations of motion has been carried out for conditions typical of gas-fluidized beds. We have only examined wave solutions which remain unchanged as they travel through the bed at constant velocity, but we will show that such an analysis is able to describe the instability of the one-dimensional waves and capture stable two-dimensional solutions that have bubble-like structure.

We chose to focus first on gas-fluidized beds, since the results of Anderson *et al.* (1995) suggest that an analysis of fully developed steady (constant shape) travelling wave solutions should suffice for this case. Their results also suggest that the treatment of liquid-fluidized beds will be considerably more complex, requiring an examination of fully developed, both spatially and temporally oscillating travelling wave solutions.

It will be shown that one-dimensional travelling wave solutions emerge through a Hopf bifurcation of the uniform state and that two-dimensional travelling waves are born out of these one-dimensional waves. It will also be seen that fully developed two-dimensional travelling wave solutions of high amplitude have bubble-like structure. The robustness of these structures will be established by exploring the effect of changes in model parameters and closures.

## 2. Equations of motion

Ensemble-averaged (or volume-averaged) equations of motion for the fluid and particle phases in fluid–particle suspensions have been described extensively in the literature, for example, see Anderson & Jackson (1967), Drew (1971), Drew & Segel (1971), Hinch (1977), Nigmatulin (1979), Joseph & Lundgren (1990), and Zhang & Prosperetti (1994). Averaged equations have been explicitly or implicitly used by many previous researchers to model the flow in fluidized beds (for example, see Jackson 1963*a*; Anderson & Jackson 1967; Garg & Pritchett 1975; Homsy *et al.* 1980; Anderson *et al.* 1995). The equations used in this work are those proposed by Anderson & Jackson (1967). Assuming an incompressible fluid and defining the following averaged variables: $\boldsymbol{v}$ the solids velocity, $\boldsymbol{u}$ the fluid velocity, $\phi$ the volume fraction of solids, $\boldsymbol{\sigma}_s$ the solid-phase stress tensor, $\boldsymbol{\sigma}_f$ the fluid-phase stress tensor, the equations of continuity and motion for the solid and fluid

phases are

$$\frac{\partial \phi}{\partial t} + \nabla \cdot [\phi \boldsymbol{v}] = 0, \tag{1}$$

$$\frac{\partial (1-\phi)}{\partial t} + \nabla \cdot [(1-\phi)\boldsymbol{u}] = 0, \tag{2}$$

$$\rho_s \phi \left[\frac{\partial \boldsymbol{v}}{\partial t} + \boldsymbol{v} \cdot \nabla \boldsymbol{v}\right] = -\nabla \cdot \boldsymbol{\sigma}_s - \phi \nabla \cdot \boldsymbol{\sigma}_f + n\tilde{\boldsymbol{f}} + \phi \rho_s \boldsymbol{g}, \tag{3}$$

$$\rho_f (1-\phi) \left[\frac{\partial \boldsymbol{u}}{\partial t} + \boldsymbol{u} \cdot \nabla \boldsymbol{u}\right] = -(1-\phi) \nabla \cdot \boldsymbol{\sigma}_f - n\tilde{\boldsymbol{f}} + (1-\phi)\rho_f \boldsymbol{g}, \tag{4}$$

where $n$ is the number of particles per unit volume, $\tilde{\boldsymbol{f}}$ is the average drag force exerted on a particle by the fluid due to the relative velocity of the phases and $\boldsymbol{g}$ is the specific gravity force vector. In the present study a Newtonian form is assumed for the fluid- and solid-phase stress tensors,

$$\boldsymbol{\sigma}_s = p_s \boldsymbol{I} - \mu_s \left[\nabla \boldsymbol{v} + (\nabla \boldsymbol{v})^T - \tfrac{2}{3}(\nabla \cdot \boldsymbol{v})\boldsymbol{I}\right], \tag{5}$$

$$\boldsymbol{\sigma}_f = p_f \boldsymbol{I} - \bar{\mu}_f \left[\nabla \boldsymbol{u} + (\nabla \boldsymbol{u})^T - \tfrac{2}{3}(\nabla \cdot \boldsymbol{u})\boldsymbol{I}\right], \tag{6}$$

where $\bar{\mu}_f$, the effective viscosity of the fluid, was assumed to be equal to $\mu_f$, the viscosity of the fluid itself. The fluid pressure, $p_f$, is determined dynamically since we have assumed the fluid to be incompressible. The particle-phase pressure, $p_s$, and effective particle-phase viscosity, $\mu_s$, need to be determined empirically or from modelling considerations. The functional forms and origin of these interactions have been the subject of some debate in the literature (Buyevich 1972; Garg & Pritchett 1975; Foscolo & Gibilaro 1984, 1987; Batchelor 1988; Mutsers & Rietema 1977; Rietema & Piepers 1990). For the moment the precise forms for $p_s$ and $\mu_s$ are not crucial for our analysis so we will take $p_s$ to be a monotonically increasing function of $\phi$,

$$p_s = g(\phi), \quad g'(\phi) > 0,$$

and the effective particle-phase viscosity will be taken to be a (non-zero) constant or monotonically increasing function of $\phi$,

$$\mu_s = h(\phi), \quad h'(\phi) \geqslant 0.$$

The drag force per unit volume, $n\tilde{\boldsymbol{f}}$, is given by bed expansion measurements or drag coefficient correlations and the following form is adopted:

$$n\tilde{\boldsymbol{f}} = (1-\phi)\beta\left(\phi, |\boldsymbol{u}-\boldsymbol{v}|\right)[\boldsymbol{u}-\boldsymbol{v}] \tag{7}$$

with

$$\frac{\partial \beta}{\partial \phi} > 0$$

where $\beta$ is also a monotonically increasing function of $\phi$. This formulation does not take into account virtual mass effects which would be expected to be negligible for gas-fluidized beds.

With the above closures there is an equilibrium solution to (1), (2) (3) and (4) which represents uniform fluidized beds of infinite extent, with

$$\phi = \phi_0\,; \quad \boldsymbol{v} = 0\,; \quad \boldsymbol{u} = \boldsymbol{j}u_0\,; \quad \nabla p = [\rho_s \phi + \rho_f (1-\phi)]\boldsymbol{g}\,; \quad \beta u_0 - \phi_0(\rho_s - \rho_f)g = 0,$$

where $\boldsymbol{j}$ is the unit vector in the $y$-direction pointing vertically upward and $\phi_0$ and $u_0$ are constants. The linear stability of this solution against small, spatially periodic one-

and two-dimensional disturbances has been examined by many researchers (Jackson 1963*a*; Murray 1965; Pigford & Baron 1965; Mutsers & Rietema 1977; Liu 1982; Foscolo & Gibilaro 1984; Batchelor 1988; Hernández & Jiménez 1991). When $\phi_0$ is smaller than some critical value, $\phi_c$, the state of uniform fluidization is linearly unstable and the fastest growing disturbance is an upward travelling wave with no horizontal structure. The wave takes the form of alternating bands of high and low voidage, which move upwards through the bed (see §3).

If the contribution of the solid-phase stress is not taken into account (see Jackson 1963*a*) then small disturbances to the uniformly fluidized bed are always linearly unstable. As recognized by Garg & Pritchett (1975) the addition to the particle-phase momentum equation of a force proportional to the spatial gradient of the particle concentration will stabilize the uniform bed, provided the force is directed from regions of high $\phi$ to low $\phi$ and the force is large enough. The particle-phase pressure provides such a force in this formulation. Since the functional form of $p_s$ is still a subject of debate we have considered a number of different functional forms. The function we have adopted for the bulk of our work is

$$p_s = g_1(\phi) = C_1 \phi^3 \exp\left[\frac{r\phi}{\phi_p - \phi}\right] \tag{8}$$

which is chosen to match a form used by Hernández & Jiménez (1991) in calculating bubble development; it represents a pressure which increases from zero when $\phi = 0$ and diverges as the solids fraction tends to the random close-packed value, $\phi_p$. It has been argued by Buyevich (1972) that for dilute beds ($\phi \to 0$) the particle pressure should be proportional to $\phi^3$, which is reflected in (8). This equation contains two constants $C_1$ and $r$, which permit the magnitude and slope of $p_s$, and hence the critical volume fraction $\phi_c$ for limiting stability to be adjusted (as will be discussed later). The value of $\phi_p$ is taken to be 0.65 (Berryman 1982).

In order to investigate the sensitivity of the results to changes in the closure for $p_s$, we considered a different closure relation, namely

$$p_s = g_2(\phi) = C_2 \frac{\phi^{m_1}}{(\phi_p - \phi)^{m_2}}. \tag{9}$$

Such a relation was employed by Johnson & Jackson (1987) in their study of granular shear flow. We analysed two cases corresponding to $(m_1 = 1, m_2 = 0)$ and $(m_1 = 1, m_2 = 2)$. The first case describing a linear variation of $p_s$ with $\phi$ has been analysed by several researchers (for example, see Needham & Merkin 1983, 1984, 1986). Note that this closure lacks the physics required to constrain the value of $\phi$ to remain below $\phi_p$ in the travelling wave solutions. The second case $(m_1 = 1, m_2 = 2)$ contains this restriction and represents a particle pressure which is proportional to $\phi$ for small $\phi$. The $p_s$-closures analysed in many previous studies (Needham & Merkin 1984; Foscolo & Gibilaro 1987; Batchelor 1988; Koch 1990) reduce to a linear variation of $p_s$ with $\phi$ as $\phi \to 0$. It can easily be shown that such a linear dependence will give rise to a region of stable uniform fluidization for sufficiently small $\phi$. On the other hand, the closure given by (8) does not yield this region of stable uniform fluidization at the dilute limit. To the best of our knowledge, the existence of a stable uniform fluidized bed at the dilute end or its absence has not been demonstrated in any experimental study. We will demonstrate in this paper that the bifurcation diagrams, for *dense* fluidized beds, obtained with these different $p_s$-closures are qualitatively similar.

The dependence of the particle-phase effective viscosity on $\phi$ is taken to have the form

$$\mu_s = h_1(\phi) = \frac{A\phi}{1 - (\phi/\phi_p)^{1/3}} \tag{10}$$

which also increases from zero when $\phi = 0$ and diverges as the solids fraction tends to $\phi_p$. The choice of a value for the parameter $A$ permits the length scale of the dominant instability of the uniform state to be adjusted. We have also considered the effect of setting $\mu_s$ to a constant value (independent of $\phi$).

The drag coefficient $\beta$ is usually correlated to the Reynolds number

$$R_t = \frac{2a v_t \rho_f}{\mu_f}$$

for a particle at its terminal velocity of fall under gravity, $v_t$. The quantity $a$ is the particle radius. At low values of $R_t$ the drag coefficient is independent of the relative velocity of the particle and fluid phases and a convenient form for a fluidized bed is

$$\beta = \frac{\phi(\rho_s - \rho_f)g}{v_t\,(1-\phi)^{(n-1)}} \tag{11}$$

which is the well known Richardson–Zaki (1954) relation with exponent $n$ depending on $R_t$. For most of the work we have carried out, the value of $R_t$ is 20, but for all of our results $R_t$ does not exceed 50. This is certainly not a low enough Reynolds number to say that the drag coefficient, $\beta$, is independent of $|\boldsymbol{u} - \boldsymbol{v}|$, but it is low enough to say that contributions from $|\boldsymbol{u} - \boldsymbol{v}|$ to $\beta$ will be small. This can be verified by considering a drag correlation such as the Ergun equation (Ergun 1952). Considering the simple forms we have adopted for $p_s$ and $\mu_s$ we will make use of (11) to approximate the drag force. The terminal velocity is calculated using empirical correlations from Kunii & Levenspiel (1991). The forms for $p_s$, $\mu_s$ and $\beta$ given in (8), (10) and (11) are those we will initially consider and were those adopted by Anderson *et al.* (1995) in their numerical simulation of flow in a fluidized bed.

Although it is straightforward to cast the equations of motion in a dimensionless form, the most appropriate characteristic length and time for the present problem is not fully understood. This has been recognized by Anderson & Jackson (1968), Garg & Pritchett (1975), Foscolo & Gibilaro (1987) and Kuipers *et al.* (1991), who have simply presented their results in terms of dimensional quantities. We note at the outset that the key features of the bifurcation diagrams described here do not depend on the choice of characteristic density, length and time, and that the results could have been presented in a dimensional form. However, we will non-dimensionalize the problem using

$$\rho_s, \quad v_t, \quad L = \left(\frac{A v_t}{\rho_s g}\right)^{1/2} \quad \text{and} \quad T = L/v_t$$

as characteristic density, velocity, length and time, respectively, and present our results in terms of dimensionless variables. The particular choice of characteristic length is motivated by the linear stability analysis of the uniform state (see Liu 1982). With this choice of characteristic scales, the following dimensionless groups are obtained:

$$\delta = \rho_f/\rho_s, \qquad \text{density ratio,}$$
$$\gamma = \bar{\mu}_f/A, \qquad \text{viscosity ratio,}$$

$$\alpha = \frac{C_1 \text{ (or } C_2)}{\rho_s v_t^2}, \qquad \text{particle-phase pressure coefficient,}$$

$$\Omega = \left(\frac{\rho_s v_t^3}{Ag}\right)^{1/2}$$

One can readily define a Reynolds number and a Froude number in terms of characteristic scales:

$$R = \frac{\rho_s v_t L}{A}, \qquad F = \frac{v_t^2}{gL},$$

and for the specific choice of $L$ employed in our study, $R = F = \Omega$. The advantage of this choice of length scale is discussed later (§7).

We limit the scope of the present study to an analysis of the solution structure for dense beds of infinite extent and seek fully developed, spatially periodic solutions propagating vertically at constant speed. Furthermore, we restrict our attention to conditions representative of gas-fluidized beds where $\delta \ll 1$ and $\gamma \ll 1$. In work on gas-fluidized beds the additional simplification of $\delta = 0$ and $\gamma = 0$ has been proposed quite often, which translates to discarding the inertial terms on the left-hand side of (4) and neglecting the deviatoric stresses in the fluid phase. Göz (1992) discusses how such a simplification could change the bifurcation scenario. We will therefore not carry out this simplification but will examine if doing so does in fact change our results.

Nominal values of model parameters used in our study are listed in table 1. They correspond to 200 μm diameter glass beads fluidized by air at ambient conditions. The constants $C_1$ and $r$ for particle pressure affect the value of the critical volume fraction $\phi_c$, and for the chosen values one obtains $\phi_c = 0.576$. The corresponding dimensionless quantities are also included in this table. We will initially fix the volume fraction of solids in the bed at a value just below the critical value and examine instabilities and solutions for this case; the chosen value is $\phi_0 = 0.57$. Subsequently, we will examine the effect of varying the mean volume fraction of particles in the bed. The parameter $A$ in the solids viscosity, $\mu_s$, is taken to be 0.5 P, which yields a value of $\mu_s^0 = 6.65$ P evaluated at $\phi_0 = 0.57$. This value is in the right range suggested by experiments. Model parameters shown in the second column of table 1, corresponding to 300 μm diameter glass beads, will be used at a later stage to show the effect of particle size on the bifurcation diagram.

The results of a linear stability analysis of the uniform state are illustrated in figure 1 where the real part of the complex growth rate of the disturbance is plotted against the vertical wavenumber $k_y$. The horizontal wavenumber, $k_x$, is zero for all the curves. For $\phi_0 > \phi_c = 0.576$ the uniform state is stable for all vertical wavenumbers. If $\phi_0 < \phi_c$ , the uniform state is unstable for a range of $k_y$ values, but is stable for large values of $k_y$. As $\phi_0$ decreases, the range of $k_y$ values for which the uniform state is unstable increases (at least in the vicinity of $\phi_c$). For all $k_y$ values, the growth rate is complex, indicating that the instability is a travelling wave (not shown).

For the purpose of our bifurcation analysis, it is convenient to summarize the linear stability results as follows. For a given value of $\phi_0 < \phi_c$, as one decreases $k_y$ from a large value where the uniform solution is expected to be stable, a pair of complex-conjugate eigenvalues cross the imaginary axis at some critical $k_y$ value. This Hopf bifurcation signals the birth of a new family of travelling wave solutions away from the uniform state. The value of this critical $y$-wavenumber where the Hopf bifurcation occurs depends on $\phi_0$, *but not on the size of the periodic box in the*

| | | |
|---|---|---|
| $\rho_s$ | 2.2 g cm$^{-3}$ | 2.2 g cm$^{-3}$ |
| $\rho_f$ | 0.0013 g cm$^{-3}$ | 0.0013 g cm$^{-3}$ |
| $\mu_f$ | 0.0181 cP | 0.0181 cP |
| $a$ | 100 μm | 150 μm |
| $v_t$ | 142 cm s$^{-1}$ | 231 cm s$^{-1}$ |
| $\phi_p$ | 0.65 | 0.65 |
| $\phi_c$ | 0.576 | 0.592 |
| $\phi_0$ | 0.57 | 0.586 |
| $A$ | 0.5 P | 0.5 P |
| $\mu_s(\phi_0)$ | 6.65 P | 8.63 P |
| $C_1$ | 1.08 Pa | 1.08 Pa |
| $r$ | 0.3 | 0.3 |
| $L$ | 0.182 cm | 0.231 cm |
| $T$ | 0.00128 s | 0.00100 s |
| $R_t$ | 20 | 50 |
| $n$ | 4.35 | 4.00 |
| $\delta$ | 0.000591 | 0.000591 |
| $\gamma$ | 0.000363 | 0.000363 |
| $\alpha$ | 0.000242 | 0.0000917 |
| $\Omega$ | 113.7 | 235.2 |

TABLE 1. Values of parameters and dimensionless groups for gas-fluidized beds. First column, 200 μm diameter glass beads; second column, 300 μm diameter.

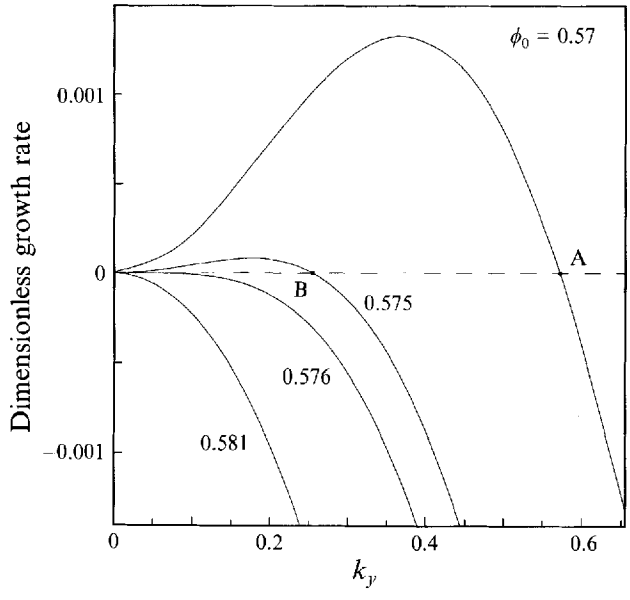


FIGURE 1. Linear stability of the uniform state. Real part of the (complex) growth rate as a function of $k_y$ for various values of $\phi_0$. $k_x = 0$.

*horizontal direction*, since the family of solutions emerging at this Hopf bifurcation consists of one-dimensional waves with variations only in the $y$-direction. We will refer to these one-dimensional travelling wave solutions as 1D-TWs and compute them numerically as described below.

## 3. One-dimensional travelling waves

Every 1D-TW is characterized by two parameters, namely, $\phi_0$ and $k_y$. Most of the discussion presented in this paper will be concerned with the family of 1D-TWs generated by holding $\phi_0$ constant and allowing $k_y$ to vary. The usual procedure to compute these 1D-TWs involves a continuation scheme starting from a known solution which is often the Hopf bifurcation point. Each 1D-TW will have its own wave speed, $c$, which needs to be determined as a part of the solution. Although this 1D-TW will appear as a time-dependent solution when viewed from an arbitrary frame of reference, it will be seen as a steady solution from an inertial frame moving at the speed of the wave. We therefore make a change of variables to a coordinate system in the travelling wave frame,

$$Y = y - ct, \quad t = t, \tag{12}$$

and seek steady solutions in this coordinate system, along with the unknown wave speed $c$. We approximate all the variables with a full Fourier series in this moving frame. Accordingly, an expansion of the type

$$\Phi_N^\theta(Y,t) = b_0^\theta(t) + \sum_{n=1}^{N} \left[a_n^\theta(t)\sin(nYk_y) + b_n^\theta(t)\cos(nYk_y)\right] \quad \text{for} \quad \theta = \phi, \tilde{p}, v_y, u_y \tag{13}$$

is used to represent the volume fraction of particles, the spatially periodic component of the fluid pressure, $\tilde{p}$, and the ($y$-component of the) velocities of both the particulate and fluid phases in the moving frame. This gives us periodicity in the $y$-direction, with period $2\pi/k_y$ for $\phi, \tilde{p}, v_y$ and $u_y$. Although all the Fourier coefficients have been shown in the above equations as time-dependent, they will become independent of time provided the speed $c$ in (12) is indeed the wave speed and the wave is fully developed and steady.

We now substitute the above Fourier expansion for all the variables into the continuity and momentum equations and form the inner product of the resulting equations with each of the $2N+1$ Fourier basis functions. The integrals are evaluated numerically through the use of the inverse discrete Fourier transform. This type of pseudospectral discretization procedure together with its convergence properties is discussed in detail by Canuto *et al.* (1988). In order to reduce aliasing errors for the nonlinear terms we use a discrete Fourier transform with $2L+1$ rather than $2N+1$ points where $L > N$. In all the results reported here, we have used $L = 5N$. The choice of such a large value for $L$ is due to the nonlinearities in the model equations and the sharp profiles we have computed. The convergence of the resulting approximation to the true solution of the model equations is tested by examining the dependence of the approximate solution on $N$. This pseudospectral approach produces a system of differential and algebraic equations for the various Fourier coefficients. A number of observations can be made immediately.

(i) It can be seen from the solids-phase continuity equation that

$$\frac{\mathrm{d}b_0^\phi}{\mathrm{d}t} = 0,$$

where $b_0^\phi$ is defined in (13) and is applied to particle volume fraction. This is to be expected as the imposition of periodic boundary conditions will necessarily constrain the average value of particle volume fraction in the cell, i.e. $b_0^\phi$ is equal to a constant at all times.

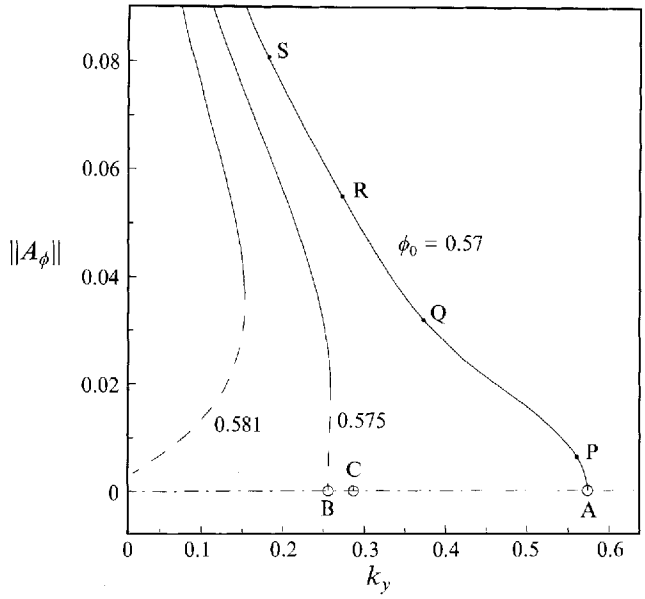


FIGURE 2. Bifurcation diagram for one-dimensional travelling waves. Volume fraction of solids norm, $\|A_\phi\|$, versus $k_y$ for various values of $\phi_0$: the uniform state (— - —), unstable 1D-TW (— — —), stable 1D-TW (———).

(ii) $b_0^{\tilde{p}}$ cannot be determined uniquely. This is not surprising as only gradients in pressure appear in the momentum equations. With no loss of generality, we set $b_0^{\tilde{p}}$ to be zero.

(iii) The mean solids velocity and mean gas velocity are given by $b_0^{v_y}(t)$ and $b_0^{u_y}(t)$ respectively, as defined in (13) (for a frame of reference moving vertically at some velocity $c$). It turns out that only $(b_0^{v_y}(t) - b_0^{u_y}(t))$ can be determined uniquely. This is hardly surprising, as it is well known that we can add any arbitrary, constant velocity to both gas and solids velocity in an unconfined fluidized bed without affecting the overall solution (due to the Galilean invariance of the equations). This makes it necessary that we choose one frame of reference for the purpose of our discussions. Accordingly, we *define* the laboratory frame as one in which the average flux of particles is zero:

$$\bar{Q}_s = \frac{1}{l_y}\int_0^{l_y} \phi(y,t)\, v_y(y,t)\, \mathrm{d}y = 0,$$

where the vertical velocity of the particles, $v_y$, is measured from the laboratory frame (and $l_y = 2\pi/k_y$ is the dimensionless wavelength in the $y$-direction). The velocity of the wave, $c$, referred to earlier is measured from this (laboratory) frame. Further mathematical details can be found elsewhere (Glasser 1995).

Figure 2 shows the particle volume fraction norm, $\|A_\phi\|$, as a function of $k_y$ for three different values of $\phi_0$. Here $\|A_\phi\|$ is based on the $L_2$ norm of the Fourier coefficients and is defined by

$$\|A_\phi\| = \left\{ \sum_{n=1}^{N} \left[ \left(a_n^\phi\right)^2 + \left(b_n^\phi\right)^2 \right] \right\}^{1/2} \tag{14}$$

This gives a measure of the amplitude of the solution with respect to the uniform

state. The mean solids volume fraction, $b_0^{\phi}(=\phi_0)$, is not included in the norm so that solutions of different $\phi_0$ can be compared. In figure 2 the base (uniform) state is represented by the dot-dashed line $\|A_\phi\| = 0$.

Consider first solutions with $\phi_0 = 0.57$. Point A in figure 2 corresponds to point A in figure 1 which was previously identified as a Hopf bifurcation point in the laboratory frame. When viewed from a moving frame which is travelling at the wave speed, a real eigenvalue will cross the imaginary axis at point A. The 1D-TW denoted by the branch APQRS (in figure 2) was computed using the steady-state part of the continuation package, AUTO (Doedel, Keller & Kernevez 1991), modified to account for the unknown speed, $c$. The modification involves adding an equation, which is used to determine the wave speed, and also eliminates the translational invariance of the solution in the wave frame. Our particular implementation of the inflation of the system of equations within the framework of AUTO is discussed by Brown & Kevrekidis (1995).

Plots of $\phi$ versus scaled height, $Y^*(= Yk_y/2\pi)$, in the travelling wave frame for 1D-TWs corresponding to points A, P, Q and S in figure 2 are shown in figure 3. The number of Fourier modes, $N$, (see (13)) used to represent each of the wave solutions, is given in the caption to figure 3. This is the minimum number of modes needed to accurately represent the solution. Small-amplitude solutions (such as curves A and P in figure 3) are nearly sinusoidal as one would expect. As we decrease the $y$-wavenumber (i.e. consider boxes of larger vertical dimension) the wave increases in amplitude and steepens (see curve Q in figure 3). It can be seen from figure 1 that the largest growth rate for $\phi_0 = 0.57$ is predicted by the linear stability analysis to occur at $k_y = 0.373$. The wave corresponding to this particular value of $k_y$ is given by curve Q in figure 3. Note that as $k_y$ decreases the $\phi$-profile becomes increasingly asymmetric as predicted and discussed previously by Fanucci *et al.* (1981), Ganser & Drew (1990), Göz (1993*a*,*b*), Dankworth & Sundaresan (1991), and Anderson *et al.* (1995).

We mention in passing that other bifurcations which are replications of the initial bifurcation are also possible on the uniform branch. Thus, for example, a family of travelling waves bifurcates out of the uniform state at point C (in figure 2) whose $y$-wavenumber is one-half of that of point A. This family of travelling waves will have two humps within one periodic cell and each of these humps will correspond exactly with a wave with twice the value of $k_y$ (emerging from point A). Similarly a three-humped wave is possible at one-third of the original wavenumber and so on. The solutions on these branches with multiple humps are initially unstable and will therefore not be discussed further here.

Let us now consider solutions in figure 2 which correspond to $\phi_0 = 0.575$. A family of 1D-TWs emerge from point B which corresponds to B in figure 1. The 1D-TW branch for this $\phi_0$ value bifurcates from the uniform state in a subcritical fashion. This branch subsequently turns around and gains stability. It is important to spell out what is meant by stability in the present context. One-dimensional travelling waves, corresponding to points on the $\|A_\phi\|$ *vs.* $k_y$ curve shown in figure 2, indicated by solid curves are stable to small one-dimensional (i.e. $y$-variation only) disturbances which retain the same periodicity as the wave itself, and have wavenumber larger than or equal to the wavenumber of the wave. The segments shown by dashed lines in this figure are unstable to such disturbances. It is interesting to note that, in every system examined in our study, the 1D-TW branch came off subcritically for $\phi_0$ values that are just below $\phi_c$ and it subsequently turned around and stabilized. This subcritical behaviour was noted by Ganser & Drew (1990), but they were not able to verify that

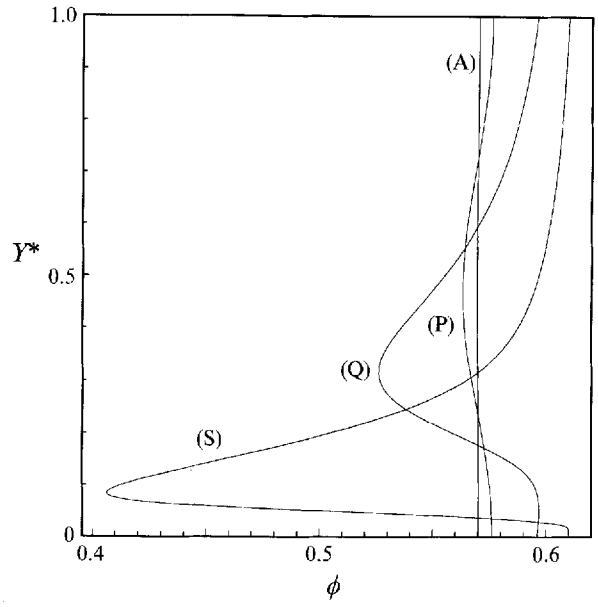


FIGURE 3. One-dimensional travelling waves corresponding to points A, P, Q and S in figure 2. $Y^* = Yk_y/2\pi$. (A) $k_y = 0.573$, $N = 4$ modes. (P) $k_y = 0.561$, $N = 6$ modes. (Q) $k_y = 0.373$, $N = 10$ modes. (S) $k_y = 0.182$, $N = 45$ modes. Curve (A) corresponds to a point on the 1D-TW branch very close to point A in figure 2.

the branch turned around. As seen from the curve APQR, this subcritical behaviour is not observed at lower values of $\phi_0$. When a subcritical bifurcation is followed by a turning point, it is seen that a stable, high-amplitude 1D-TW coexists with a stable uniform state for a range of $k_y$ values.

It is clear from figure 2 that as we increase $\phi_0$ the bifurcation of 1D-TWs from the uniform state occurs at smaller and smaller $k_y$ values. When $\phi_0 = \phi_c$ this bifurcation occurs at $k_y = 0$, as discussed in detail by Göz (1993*a*). It can be anticipated from figure 2 that this bifurcation at $k_y = 0$ for $\phi_0 = \phi_c$ will be initially subcritical followed by a turning point. It can be inferred from this pattern of bifurcation diagrams that one-dimensional travelling wave solutions are possible for some $\phi_0$ values greater than $\phi_c$. This is illustrated in figure 2 by the curve corresponding to $\phi_0 = 0.581$. This family of 1D-TWs does not emerge through a bifurcation from the uniform state; instead, it is present as an *isolated* branch of solutions. Stable 1D-TWs in this locus will be achieved when a disturbance of sufficiently high amplitude and appropriate periodicity is imposed on the uniform state and the wave is allowed to evolve (Dankworth & Sundaresan 1991; Anderson *et al.* 1995).

## 4. Mathematical preliminaries for two-dimensional solutions

It has been already pointed out in the literature (Dankworth & Sundaresan 1991; Anderson *et al.* 1995) that the one-dimensional travelling waves obtained in the cases of gas- and liquid-fluidized beds are qualitatively similar. Therefore, one must investigate the structure of two-dimensional travelling waves in order to seek an explanation for the qualitative difference seen in the evolution of unsteady structures in gas- and liquid-fluidized beds (Anderson *et al.* 1995). The remainder of this paper will be devoted to two-dimensional travelling waves in gas-fluidized beds. When

spatial variations are permitted to occur in two dimensions, the equations permit both vertically travelling waves and oblique travelling waves (Göz 1992,1993*a*). It is clear from the past experimental studies that it must be possible to make a distinction between the gas- and liquid-fluidized beds purely on the basis of vertically travelling waves. Indeed, numerical integration of the transient continuity and momentum equations for the two phases carried out by Anderson *et al.* (1995) reveal fundamental differences between the gas- and liquid-fluidized beds even when attention is restricted to vertically travelling waves with two-dimensional structure. Accordingly, we will also restrict attention to vertically travelling waves. It will be seen shortly that the vertically travelling waves with two-dimensional structure (henceforth two-dimensional vertical travelling waves, or simply 2D-TWs) which we compute are fully developed and move at constant speed. Therefore, it is convenient to view these 2D-TWs from a coordinate system in the travelling wave frame by substituting

$$x = x, \quad Y = y - ct, \quad t = t \tag{15}$$

and computing them as steady solutions in this coordinate system. This is analogous to what we described earlier in the context of 1D-TWs.

A general Fourier series approximation for any variable which is periodic in both $x$ and $Y$ can be written as follows:

$$\begin{aligned}\Psi^{\theta}_{N,M}(x,Y,t) = {} & b^{\theta}_{0,0}(t) + \sum_{n=1}^{N}\left\{a^{\theta}_{n,0}(t)\,\sin(nYk_y) + b^{\theta}_{n,0}(t)\,\cos(nYk_y)\right\} \\ & + \sum_{m=1}^{M}\left[b^{\theta}_{0,m}(t) + \sum_{n=1}^{N}\left\{a^{\theta}_{n,m}(t)\,\sin(nYk_y) + b^{\theta}_{n,m}(t)\,\cos(nYk_y)\right\}\right]\cos(mxk_x) \\ & + \sum_{m=1}^{M}\left[d^{\theta}_{0,m}(t) + \sum_{n=1}^{N}\left\{c^{\theta}_{n,m}(t)\,\sin(nYk_y) + d^{\theta}_{n,m}(t)\,\cos(nYk_y)\right\}\right]\sin(mxk_x). \end{aligned} \tag{16}$$

The first group of terms on the right-hand side of the above equation corresponds exactly to the group considered earlier in the context of one-dimensional travelling waves. The second and third groups of terms corresponding to $\cos(mxk_x)$ and $\sin(mxk_x)$ respectively, then determine the transverse structure. We suppress the oblique travelling waves in this paper by discarding the third group of terms in our approximation for the volume fraction of particles, the $y$-component of the velocities of both the solid and fluid phases, and the spatially periodic component of the fluid-phase pressure, and by retaining only the third group of terms in our approximation for the $x$-component of the fluid and solid phase velocities.

The issue of the laboratory frame will come up once again (see earlier discussion in the context of one-dimensional waves). Retaining the same definition of the laboratory frame as before, we set

$$\bar{Q}_s = \frac{1}{l_x l_y}\int_0^{l_y}\int_0^{l_x} \phi(x,y,t)\,v_y(x,y,t)\,\mathrm{d}x\,\mathrm{d}y = 0 \tag{17}$$

where the velocity, $v_y$ of the particle phase is measured from the laboratory frame. The dimensionless wavelengths in the $y$- and $x$-directions are given by $l_y\,(=2\pi/k_y)$ and $l_x\,(=2\pi/k_x)$ respectively.

A system of differential and algebraic equations for the Fourier coefficients is obtained following the same procedure discussed earlier for one-dimensional waves. Although all the Fourier coefficients have been written as time-dependent quantities

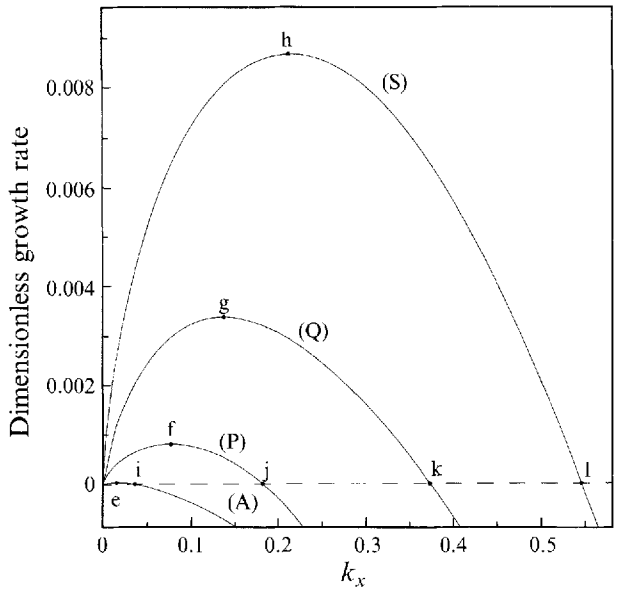


FIGURE 4. Linear stability of fully developed one-dimensional travelling waves, for $\phi_0 = 0.57$. Dimensionless growth rate as a function of $k_x$. (A) $k_y = 0.573$, (P) $k_y = 0.561$, (Q) $k_y = 0.373$, (S) $k_y = 0.182$. The 1D-TWs corresponding to curves (A), (P), (Q) and (S) are shown in figure 3.

(see (16)), they will again be independent of time if the speed of the travelling frame in (15) is indeed the wave speed and if the wave is fully developed and steady.

## 5. Stability of 1D-TWs to two-dimensional perturbations

The one-dimensional travelling waves with horizontal wave fronts, described earlier, are a special case of the solutions with two-dimensional structure and they exist for every value of $k_x$. Therefore it is natural to start our investigation with an analysis of the linear stability of a 1D-TW to small disturbances which possess the same $y$-periodicity as the 1D-TW itself and are also periodic in the $x$-direction. Such a disturbance is obtained from the second or third group of terms in (16) (which, as discussed earlier, depends on the variable $x$) by setting $M = 1$.

The results of such a linear stability analysis are illustrated in figure 4 where the growth rate of the disturbance is plotted against $k_x$, for four different 1D-TWs. These 1D-TWs correspond to four different values of $k_y$, but all of them belong to the same ($\phi_0 = 0.57$) family. Curve P in figure 4 with $k_y = 0.561$ corresponds to point P in figure 2. (The corresponding 1D-TW is shown in figure 3.) It can be seen from figure 4 that this 1D-TW is stable for large values of $k_x$, as it should be. As we decrease $k_x$, loss of stability occurs at point j where one real eigenvalue crosses zero and becomes positive (if we view the 1D-TW from a frame of reference travelling at the speed of the wave). This signals the birth of a new family of travelling wave solutions which, unlike the 1D-TWs, will possess two-dimensional structure. It will be shown later that these travelling waves (which we labelled earlier as 2D-TWs) include bubble-like solutions.

Note that as we decrease $k_x$ past point j, the growth rate increases at first reaching a maximum at point f and then decreases to zero as $k_x \to 0$. The growth rates corresponding to curves Q and S in figure 4 pertain to 1D-TWs at points Q and S

in figure 2. (The corresponding 1D-TWs are shown in figure 3.) Curve A in figure 4 corresponds to a 1D-TW of so small an amplitude that it can be captured accurately with a single Fourier mode in the $y$-direction. This 1D-TW with a $k_y$ of 0.573 is located very close to point A in figure 2. In every curve shown in figure 4, the loss of stability of the 1D-TW is associated with a real eigenvalue crossing zero. It is therefore clear that the transverse instability of the 1D-TWs is a robust feature.

The eigenfunctions corresponding to the most unstable eigenvalues for the four 1D-TWs (marked by points e, f, g and h in figure 4) are presented in figures 5 to 8. In each of these figures, the spatial variation of $\phi$ in the corresponding 1D-TW is shown as panel ($a$) in order to facilitate our discussion of the eigenfunctions. The eigenfunctions associated with particle volume fraction, fluid-phase velocity and particle-phase velocity are shown as panels ($b$), ($c$) and ($d$), respectively. Each of these panels displays spatial variation over one periodic cell of height $2\pi/k_y$ and width $2\pi/k_x$. Even though the ratio of the vertical to lateral wavenumbers is not unity, the eigenfunctions are plotted in a square box and the scaling is obvious.

It is clear from figure 5($b$) that in the case of a 1D-TW with a very small amplitude the $\phi$-perturbation is cellular with equally spaced contours and shades of grey. Figure 6($b$) associated with a somewhat higher-amplitude 1D-TW reveals slight asymmetry in the $y$-direction. It is seen in figures 5($c$) and 6($c$) that perturbations in the fluid velocity fields have their major component in the vertical direction, so these assume the form of alternating columns of upward and downward moving fluid which change direction every half wavelength in the $x$-direction. The $x$-component of the fluid velocity perturbation is very small compared to that in the $y$-direction. The character of the perturbations in the particle-phase velocity fields, shown in figures 5($d$) and 6($d$), is similar to that of the fluid phase.

The eigenfunctions corresponding to 1D-TWs of higher amplitude are shown in figures 7 and 8. It is apparent from figures 7($b$) and 8($b$) that the $\phi$-perturbations are now asymmetric (in the $y$-direction) and are confined to regions of low $\phi$ in the 1D-TWs. It can also be seen from figures 5($b$) to 8($b$) that the regions where the $\phi$-perturbation has most structure (i.e. largest variations in $\phi$) in the vertical direction, correspond to regions where the 1D-TW has the most variation in $\phi$. The lateral components of the perturbations in the fluid and solid velocity fields increase progressively as the amplitude of the 1D-TW increases.

So far we have discussed only the eigenfunctions for the lateral wavenumber corresponding to the maximum growth rate. It is instructive to examine the eigenfunction for a particular 1D-TW as the lateral wavenumber is changed. An inspection of the eigenfunctions describing $\phi$-perturbations as we move along curve P in figure 4 reveals that their 'phase' changes progressively. (Here phase of an eigenfunction refers to a shift in the eigenfunction up or down relative to the 1D-TW.) The effect of this phase change is illustrated in figure 9 which shows two $\phi$-structures obtained by adding a small amount of the $\phi$-perturbation to the 1D-TW (curve P in figure 3). The $\phi$-structures are plotted in a square box, even though the ratio of the vertical to lateral wavenumbers is not unity. Figures 9($a$) and 9($b$) correspond to points f and j, respectively, in figure 4. The 'buckling' type of structure presented in figure 9($a$) has been analysed previously by Batchelor & Nitsche (1991) and Batchelor (1993). Figure 9($b$) shows that another type of structure, namely bulging, is also possible.

It was pointed out by Anderson *et al.* (1995) that the relative magnitudes of the growth rates of the disturbances leading to 1D-TWs from the uniform state and 2D-TWs from the 1D-TWs is an important consideration in distinguishing bubbling and non-bubbling systems. It is seen from figure 1 that the fastest growing

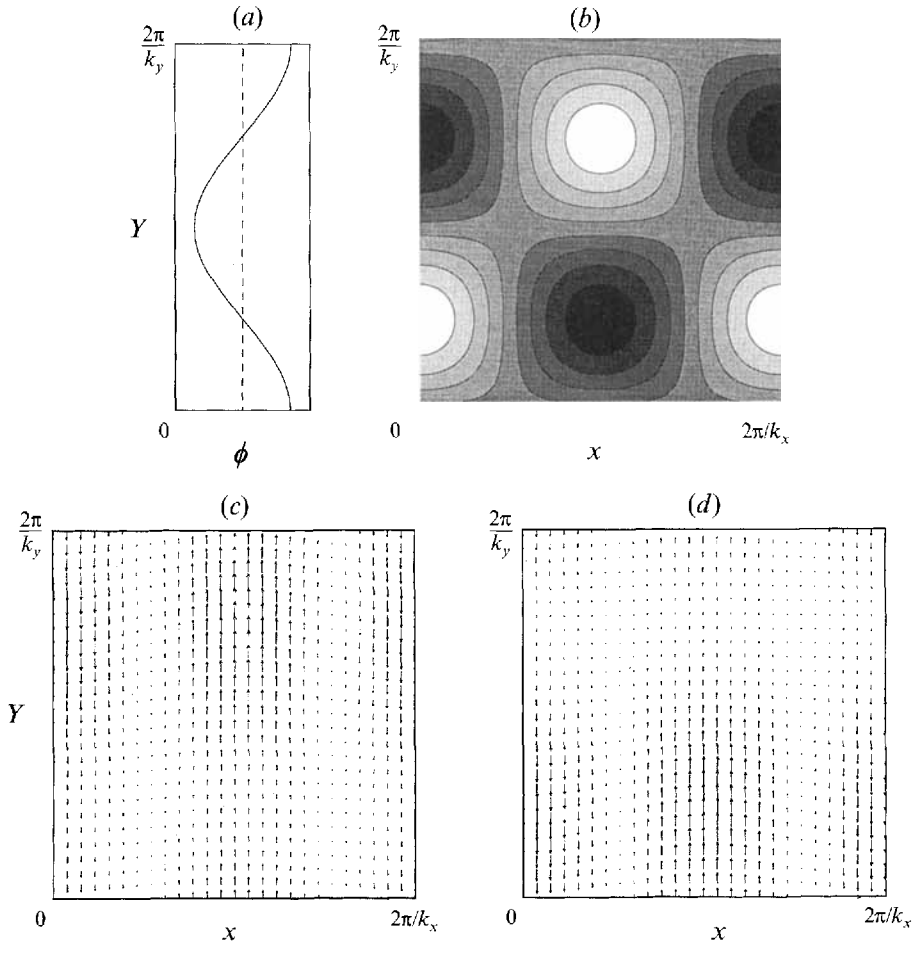


FIGURE 5. Eigenfunctions corresponding to maximum growth rate (point e) of curve (A) in figure 4. $k_y = 0.573, k_x = 0.015$. $N = 4, M = 1$. (*a*) The corresponding one-dimensional travelling wave, height versus volume fraction of solids (see figure 3 for quantitative information). The broken line shows the mean volume fraction of solids, $\phi_0 = 0.57$. (*b*) Grey-scale plot of the eigenfunction corresponding to the volume fraction of solids. The increments between shades of grey are equal. (*c*) Vector plot of gas-velocity eigenfunction. (*d*) Vector plot of solids-velocity eigenfunction. Although the eigenfunctions are shown in a square box, the actual periodic box has unequal $k_x$ and $k_y$.

disturbance away from the uniform state, $\phi_0 = 0.57$, corresponds to $k_y = 0.373$ and its dimensionless growth rate is 0.00128. Linear stability analysis of a 1D-TW with $k_y = 0.373$ reveals that two-dimensional structures will evolve from this wave at a maximum growth rate of 0.00333 (point g in figure 4). These two growth rates (0.00128 and 0.00333) are of the same order of magnitude.

## 6. Two-dimensional travelling waves

Figure 10 shows the volume fraction norm, $\|A_\phi\|$, as a function of $k_y$, where we have set $k_x = k_y$. Included in this figure are the uniform state (depicted by the line $\|A_\phi\| = 0$), the 1D-TW branch (curve APQR), and the 2D-TW branch (curve

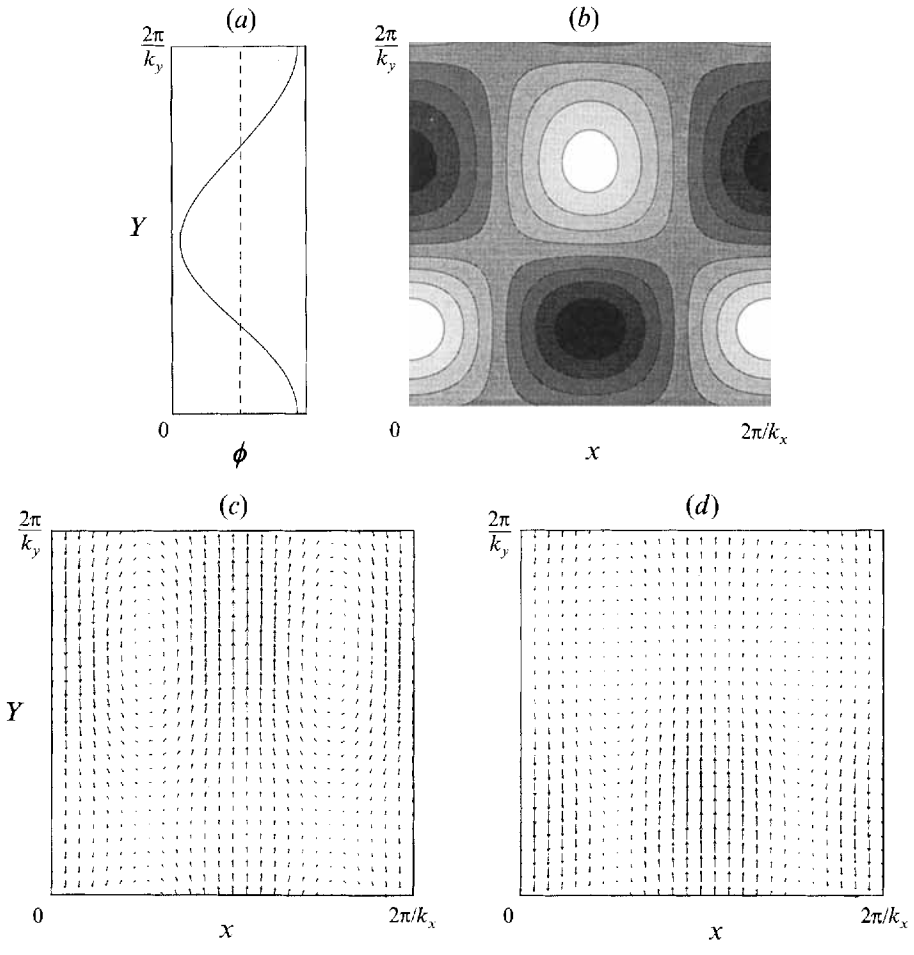


FIGURE 6. Eigenfunctions corresponding to maximum growth rate (point f) of curve (P) in figure 4. $k_y = 0.561, k_x = 0.078$. $N = 6, M = 1$. See figure 5 for description.

QLMNO). Here $\|A_\phi\|$ is defined as

$$\|A_\phi\| = \left\{ \sum_{m=1}^{M} \left(b_{0,m}^{\phi}\right)^2 + \sum_{n=1}^{N} \sum_{m=0}^{M} \left[ \left(a_{n,m}^{\phi}\right)^2 + \left(b_{n,m}^{\phi}\right)^2 \right] \right\}^{1/2}$$

and as discussed before, $b_{0,0}^{\phi} (= \phi_0)$, is not included in the norm so that solutions of different $\phi_0$ can be compared.

The 1D-TW branch (APQR in figure 10) is initially stable (for decreasing $k_y$). As we follow the solutions on this branch in the wave frame, one real eigenvalue passes through zero at point Q. In the wave frame, this is a stationary bifurcation, more specifically a pitchfork bifurcation, and the two branches that are born represent the same state with a phase shift of $\pi/k_x$ in the $x$-direction. Both these solutions have identical $\|A_\phi\|$, so they cannot be differentiated in figure 10. From a physical point of view these solutions are one and the same, so we will not differentiate between the two. The new branch that is born, QLMNO, comes off the 1D-TW branch subcritically and is initially unstable. It turns around and gains stability shortly after point L. The solutions on this new branch have a two-dimensional structure and

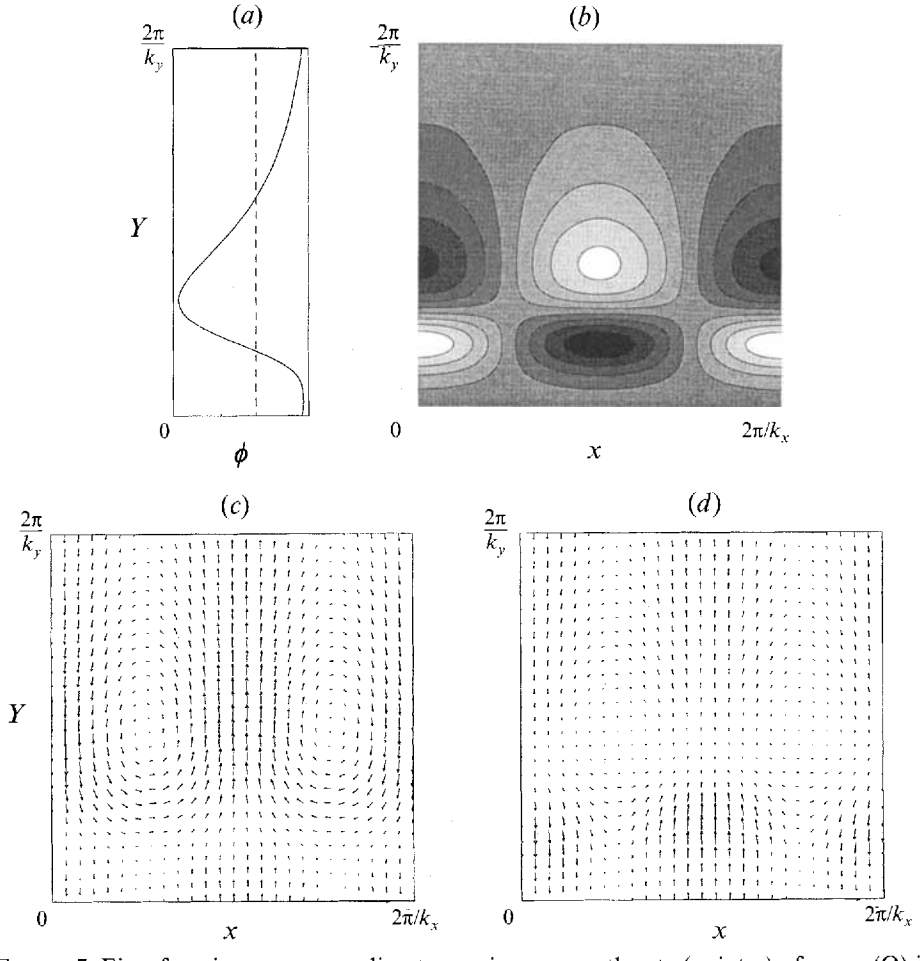


FIGURE 7. Eigenfunctions corresponding to maximum growth rate (point g) of curve (Q) in figure 4. $k_y = 0.373, k_x = 0.138$. $N = 10, M = 1$. See figure 5 for description.

still travel vertically up through the bed at constant wave speeds. Therefore, it is indeed appropriate to refer to them as two-dimensional travelling waves (2D-TWs). Examination of a solution on the 2D-TW branch just past the bifurcation point Q reveals the bulging of the 1D-TW solution (at Q) in the lateral direction. This can be seen in figure 11 plotted in the wave frame. The number of Fourier modes, $N, M$ (see (16)) used to represent the wave solution is given in the caption to the figure. The $\phi$-structure shown in figure 11($a$) is similar to that in figure 9($b$). The streamlines for the solid and gas phases show minimal departure from the vertical trajectories of the 1D-TW. Figure 12 shows a higher-amplitude 2D-TW solution which corresponds to point L in figure 10. The solid-phase streamlines are still nearly vertical (and pointing down) while a bending of the gas streamlines around the 'hole' (the region of low volume fraction of solids) is now clearly visible.

The solution at point M, which is further along the 2D-TW branch, and beyond the turning point in figure 10, is shown in figure 13. An increase in the amplitude of the $\phi$-structure (i.e. a deeper hole), the appearance of a recirculation pattern in the gas streamlines and the slight bending of the particle-phase streamlines around the hole are now evident. These features become more and more prominent as we

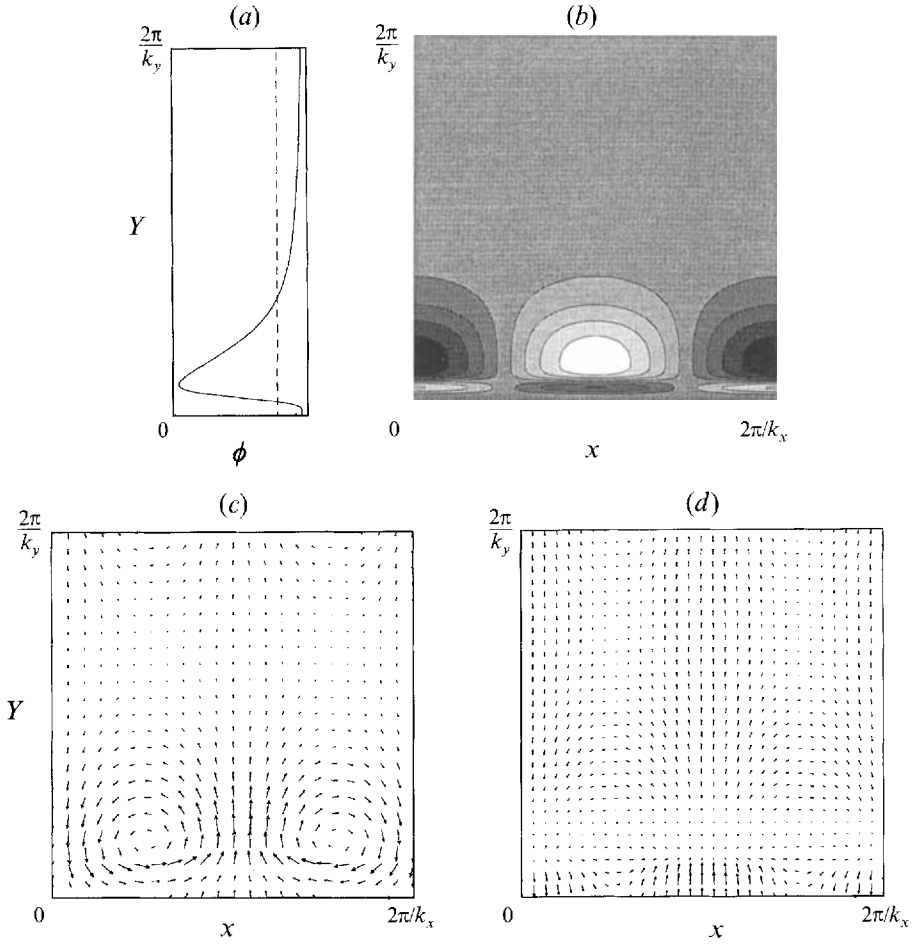


FIGURE 8. Eigenfunctions corresponding to maximum growth rate (point h) of curve (S) in figure 4. $k_y = 0.182, k_x = 0.213$. $N = 45, M = 1$. See figure 5 for description.

move up along the 2D-TW branch to point N and then to point O (see figures 14 and 15). Notice that the lowest value of $\phi$ seen in the periodic box steadily decreases as we move up along the 2D-TW branch. It seems reasonable to conclude that if we continue further up this branch we will see a bubble with little or no solids in it. Although we have calculated 2D-TW solutions up to $k_y = k_x = 0.182$ (with $N = 27$ and $M = 16$) where the volume fraction of solids inside the hole drops down to 0.05, the resolution of this wave is not entirely satisfactory. Therefore we will not present this calculation. The problem with calculating solutions as $k_x(= k_y)$ is decreased is that more and more Fourier modes are needed to accurately represent the solution. The number of Fourier modes that we can use is limited by the extent of our computational resources. Structures that are obtained with an inadequate number of Fourier modes have oscillations on the length scale of the highest Fourier modes and clearly have not converged to the true solution.

The velocities of the travelling wave solutions (in figure 10) relative to the laboratory frame are presented in figure 16 as curves PQR (for the 1D-TW) and QLMNO (for the 2D-TW). As the amplitude of the 1D-TW increases, the wave velocity increases rapidly at first and then it levels off. The velocity of the 2D-TWs decreases at first

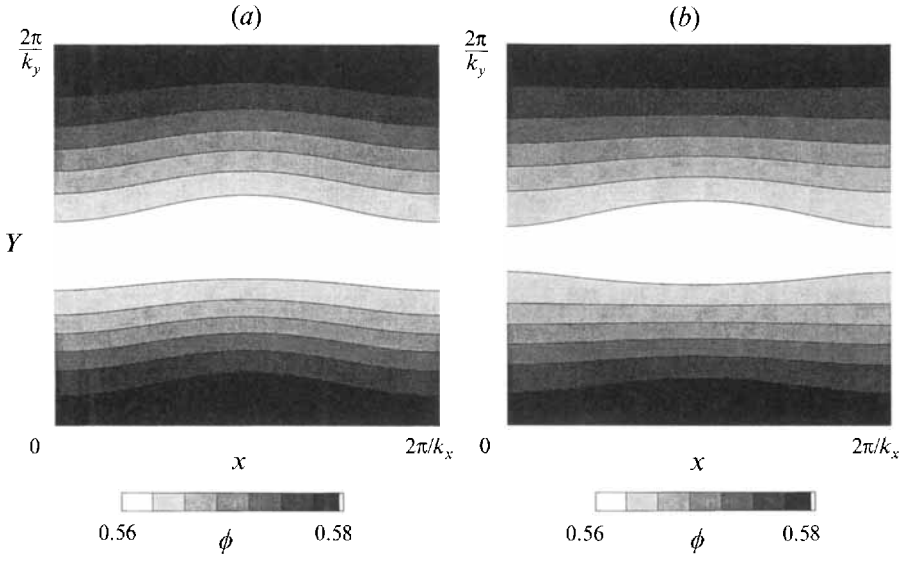


FIGURE 9. Grey-scale plot of volume fraction of solids obtained by adding a small amount of the unstable $\phi$-eigenfunction to the 1D-TW solution. The 1D-TW has $k_y = 0.561$, and is shown as curve (P) in figure 3. (*a*) $k_x = 0.078$. $N = 6, M = 1$. Eigenfunction is shown in figure 6. (*b*) $k_x = 0.182$. $N = 6, M = 1$. Eigenfunction is not shown. Numbers on the legend refer to the minimum and maximum value of $\phi$. The increments between shades of grey are equal.

(in the subcritical region); but this trend reverses past the turning point and the wave velocity continues to rise as the amplitude increases. It can be seen from figure 16 that wave velocity generally increases as $k_y (= k_x)$ decreases.

A few additional observations can be made from figure 15. Note that the hole in this figure has a diffuse roof and a rather sharp floor. The presence of a diffuse roof has been predicted previously (Jackson 1963*b*; Anderson *et al.* 1995) and observed experimentally (Lockett & Harrison 1967; Nguyen, Leung & Weiland 1973; Yates, Cheesman & Sergeev 1994). Yates *et al.* (1994) also found that the wake was a region of lower particle concentration, in contrast with the $\phi$-plot in figure 15. Also, the shape of the hole in this figure is not consistent with bubble shapes observed in two-dimensional fluidized beds. In particular, the typical upward bulge of the floor of the bubble seen in experiments is not observed. We will return to this point later on. The centre of the vortex lies somewhat above the region of lowest particle concentration (see figures 15*a* and 15*b*) as is observed experimentally.

In order to investigate the effect of the aspect ratio of the box on the 2D-TW solutions, we performed continuations for various fixed lateral wavenumbers. The volume fraction norm, $\|A_\phi\|$, is shown as a function of $k_y$ in figure 17, where we have kept $k_x$ constant at 0.182. It is this choice of $k_x$ which distinguishes this figure from figure 10 discussed earlier. The uniform state and the 1D-TW in this figure are the same as those in figure 10. The 2D-TWs are different as a result of the difference in the choice of $k_x$. In figure 17, the 2D-TW branch comes off supercritically from the 1D-TW branch at point P. This 2D-TW branch quickly turns around and loses stability. Another turning point is encountered at point X where the 2D-TW branch regains stability. The solutions (in particular, the $\phi$-structure and the gas-phase streamlines) corresponding to four different points (T, U, V and W) on the 2D-TW branch (of figure 17) are presented in figure 18. The aspect ratio of each periodic box shown in these figures retains the correct $k_y/k_x$ ratio. The evolution of the $\phi$-structure

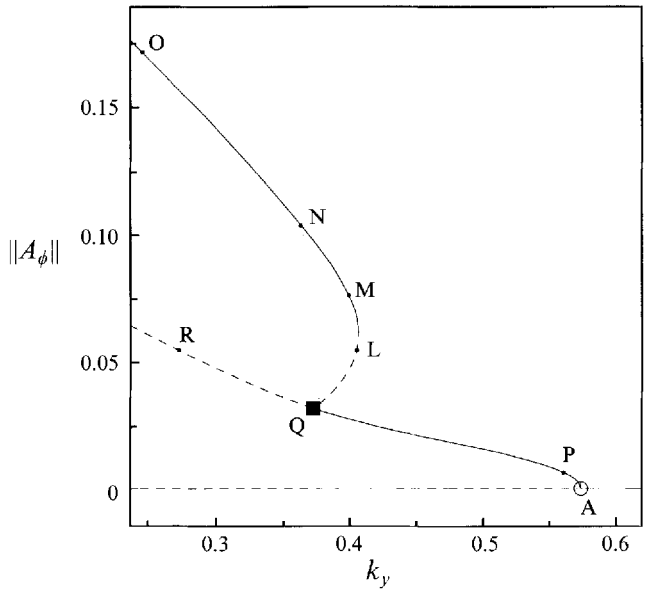


FIGURE 10. Bifurcation diagram showing the uniform state and one- and two-dimensional travelling wave solutions. $\phi_0 = 0.57$. $k_x = k_y$. The solid curves indicate stable branches. The broken curves indicate unstable branches. P,Q and R on the 1D-TW branch correspond to their namesakes in figure 2.

as one moves along the 2D-TW branch is similar to that seen earlier in figures 11 to 15. The fluid streamlines in figure 18, however, reveal an interesting difference which is worth noting. The shapes of the gas streamlines shown in figures 18(*b*) and 18(*d*) are qualitatively similar to those seen earlier in figures 12(*b*) and 14(*b*). In both figures 14(*b*) and 18(*d*), one can see two stagnation points located on the centreline. In figure 14(*b*), the stagnation point above the hole is far away from the stagnation point below the hole from the periodic box above. As a result, there is very little interaction between these two holes, as evidenced by the nearly vertical streamlines between them. In contrast, one can readily appreciate the interaction between the two holes in figure 18(*d*). On moving further up the 2D-TW branch in figure 17, the two holes interact more strongly (see figure 18*f*). The two stagnation points originally located on the centreline have now collided and moved apart in the transverse direction. The gas streamline along the centreline in figure 18(*f*) is pointing upward everywhere, which is qualitatively different from the structure in figure 18(*d*). As we move further up in the 2D-TW branch (which is tantamount to increasing the $y$-dimension of the periodic cell), the stagnation points retrace their path and return to the centreline (figure 18*h*). We have verified that interaction of the type displayed in figure 18(*f*) is not unique to $k_x = 0.182$. Such an interaction between stagnation points is known to be a precursor to bubble–bubble interactions (Clift *et al.* 1972).

The shape of a deep hole in a square periodic box is roughly circular as can be seen in figure 15(*a*) . When the aspect ratio of the periodic box is not unity a deep hole remains roughly circular as can be seen in figure 18(*g*). Thus it appears that while the shape of shallow holes reflects the aspect ratio of the box, the deep holes select a fairly circular shape, independent of this aspect ratio. The size of the hole is influenced more strongly by the smaller of the two dimensions of the periodic box.

The possibility of coexistence of stable solutions of different structure can be seen in figure 10 which shows that 1D-TWs and 2D-TWs can coexist over a range of $k_y$ values.

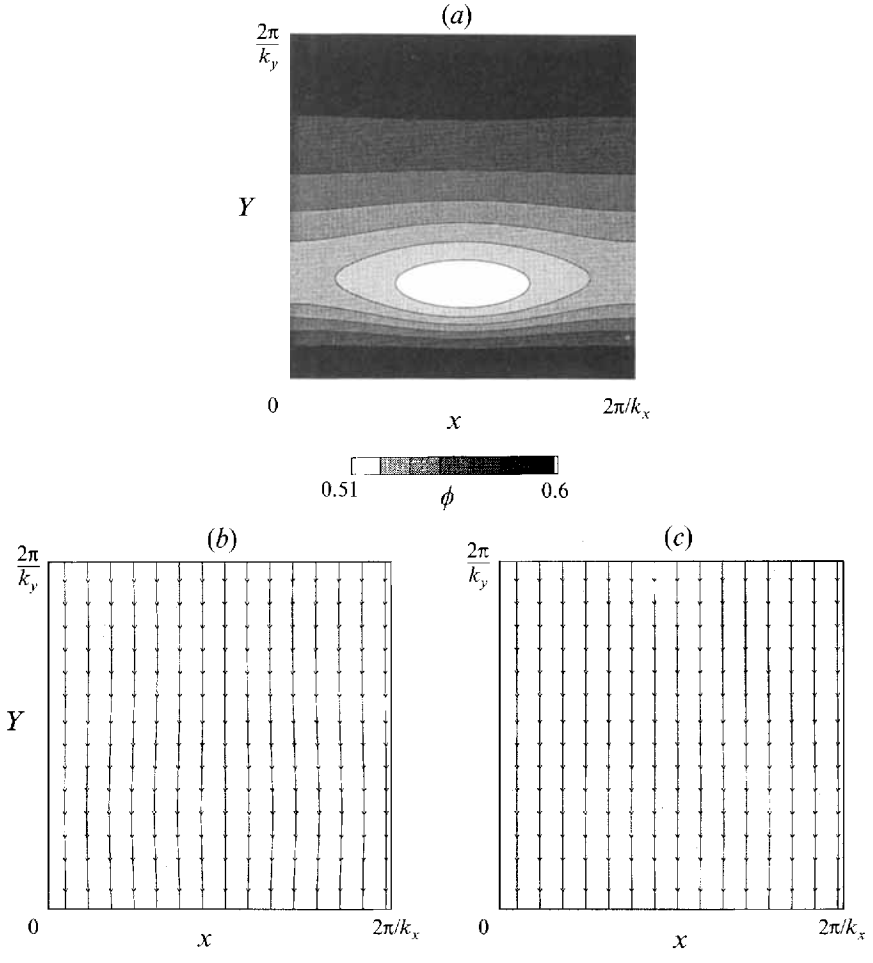


FIGURE 11. Two-dimensional travelling wave solution, near (indistinguishable from) point Q in figure 10. $k_x = k_y = 0.379$. $N = 7, M = 5$. (*a*) Volume fraction of solids. (*b*) Streamline plot of gas velocity. (*c*) Streamline plot of solids velocity.

In figure 17 such coexistence is also seen and a low-amplitude and a high-amplitude 2D-TW coexist over a narrow range of $k_y$ values. Perhaps the most interesting feature is the coexistence of a stable uniform state and a stable high-amplitude 2D-TW for some $k_y$ values.

As mentioned earlier, the 2D-TW branch comes off the 1D-TW branch subcritically in figure 10, but supercritically in figure 17. We have computed the bifurcation diagrams for several different values of $k_x$ and found that, when $k_x$ is held constant at a small value, the 2D-TW comes off supercritically from the 1D-TW. However, for larger values of $k_x$, this bifurcation occurs subcritically. For example, the bifurcation diagram for $k_x = 0.364$ is similar to figure 10. Thus the character of the initial bifurcation of the 2D-TW branch from the 1D-TW branch is strongly dependent on the choice of parameters. However, the presence of stable, high-amplitude 2D-TW solutions is a robust phenomenon.

A number of other bifurcations occur on the uniform branch, and we have already referred to multi-peaked 1D-TWs. There are also bifurcating solutions which immediately possess both vertical and lateral structure. These solutions, referred to

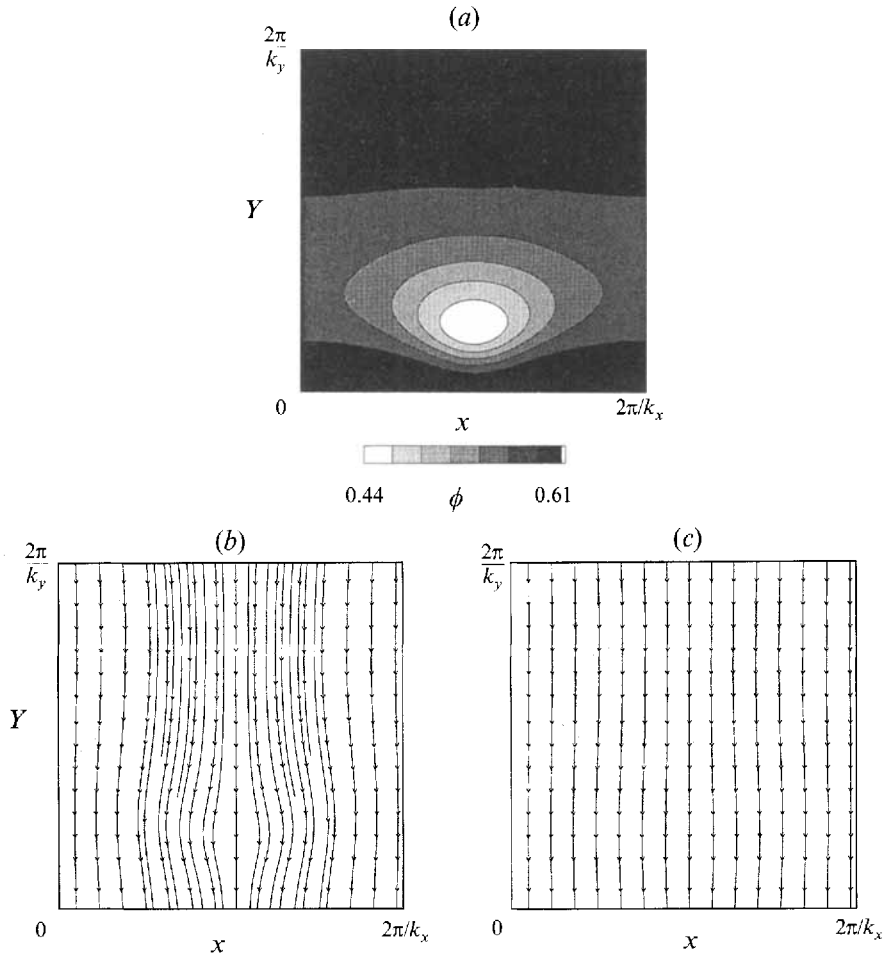


FIGURE 12. Two-dimensional travelling wave solution corresponding to point L of figure 10. $k_x = k_y = 0.406$. $N = 7, M = 5$. (*a*) Volume fraction of solids. (*b*) Streamline plot of gas velocity. (*c*) Streamline plot of solids velocity.

as standing travelling waves by Göz (1992), are born unstable at their respective bifurcation points. We have carried out continuations of such branches (see Glasser 1995) but the solutions have remained unstable (for the cases we examined) and consequently we will not describe them here. We have computed bifurcation diagrams such as figure 10 for several other values of $\phi_0$. We simply note that figures 10 and 17 are quite typical of what we found.

Figures 19(*a*) and 19(*b*) show diagrams obtained by using $\phi_0$ as the bifurcation parameter. Figure 19(*a*) corresponds to $k_y = 0.364$ and $k_x = 0.182$, while for figure 19(*b*) $k_x = k_y = 0.182$. Let us consider figure 19(*a*) first. As one decreases $\phi_0$, the uniform state loses stability at point A and a 1D-TW is born at this point. This 1D-TW branch is shown by the curve ACFD. The wave speed of the 1D-TW decreases as the mean volume fraction in the bed decreases (i.e. as one moves from C to D). The 1D-TW branch loses stability at point C and a 2D-TW branch emerges subcritically from this point. This 2D-TW branch subsequently turns around at E and stabilizes. This bifurcation diagram is similar to figure 17, although the bifurcation parameter is different. As was seen for the solutions on the 1D-TW branch the wave

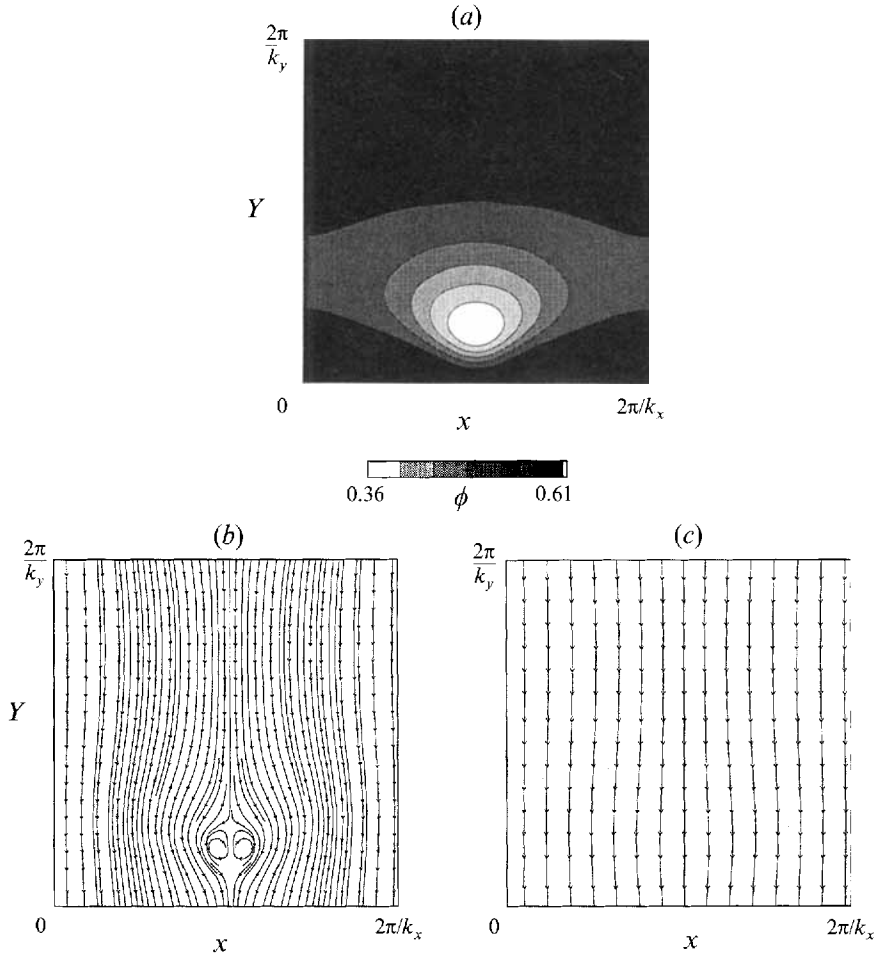


FIGURE 13. Two-dimensional travelling wave solution corresponding to point M of figure 10. $k_x = k_y = 0.400$. $N = 9, M = 7$. (*a*) Volume fraction of solids. (*b*) Streamline plot of gas velocity. (*c*) Streamline plot of solids velocity. Note: all streamlines in this figure and later figures should connect. Those streamlines that suggest spirals or disconnected segments are artifacts of our plotting routine.

speed of solutions on the 2D-TW branch decreases as the mean volume fraction in the bed decreases. Point W in figure 19(*a*) corresponds to its namesake in figure 17 and the wave is shown in figures 18(*g*) and 18(*h*). The coexistence of different types of solutions is seen in figure 19(*a*). Note that high-amplitude 2D-TWs are possible even for $\phi_0 > \phi_c$. In other words, even when the uniform state is linearly stable to perturbations *of all length scales* there can still exist stable 2D-TWs. Figure 19(*b*) is analogous to figure 10. Point N in figure 19(*b*) corresponds to its namesake in figures 10 and 16, and the wave is shown in figure 14.

## 7. Robustness of the bifurcation diagrams

Our discussion thus far has focused on a single system (200 μm diameter glass beads in air) and specific closures for $p_s$ and $\mu_s$. It is important to check the robustness of the bifurcation diagram by considering different gas–particle systems as well as other closures. This is particularly important as bubbles are formed easily in gas–fluidized

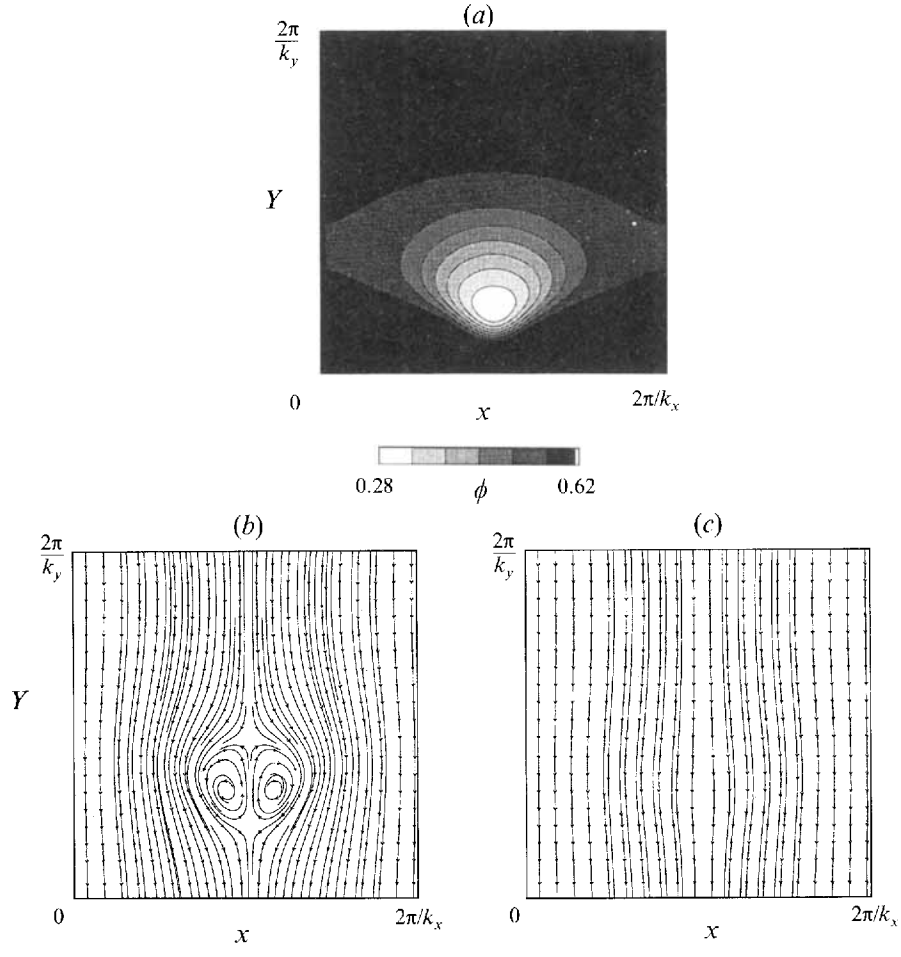


FIGURE 14. Two-dimensional travelling wave solution corresponding to point N of figure 10. $k_x = k_y = 0.364$. $N = 18, M = 10$. (*a*) Volume fraction of solids. (*b*) Streamline plot of gas velocity. (*c*) Streamline plot of solids velocity.

beds and therefore the ability to observe them in mathematical models should not be restricted to a specific set of speculative closures or parameters.

We carried out a large series of numerical experiments by changing the model parameters and the closures, and found the bifurcation diagram to be robust in the following sense: the 1D-TWs having only vertical structure emerge through a Hopf bifurcation of an unstable uniform state and the 2D-TWs are born out of these 1D-TWs. The high-amplitude 2D-TWs resemble bubbles in fluidized beds. The specific choice of closure influences the shape of the travelling wave solutions. Model parameters and choice of closures affect whether the bifurcations occur supercritically or subcritically.

As $\delta << 1$ (the density of the particles is much larger than that of the gas) one can anticipate that discarding the inertial terms on the left-hand side of (4) will have a negligible effect on the bifurcation diagram. We have indeed verified this, and found that the bifurcation diagrams obtained (using parameters in the first column of table 1) with and without the fluid-phase inertial terms are nearly identical. In a similar fashion we found that neglecting the deviatoric stresses in the fluid phase (by setting $\gamma$

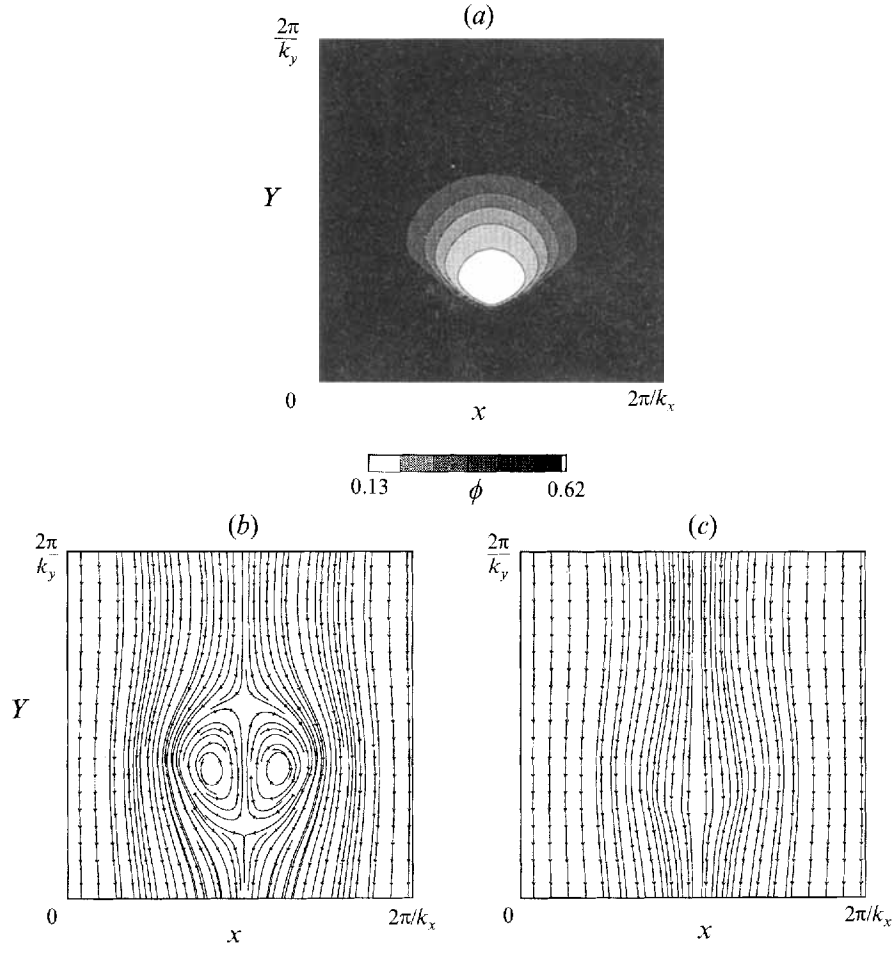


FIGURE 15. Two-dimensional travelling wave solution corresponding to point O of figure 10. $k_x = k_y = 0.246$. $N = 36, M = 24$. (*a*) Volume fraction of solids. (*b*) Streamline plot of gas velocity. (*c*) Streamline plot of solids velocity.

equal to zero which is equivalent to setting $\bar{\mu}_f$ equal to zero in (6)) had no discernible effect on the bifurcation diagram.

The dimensionless groups or parameters, $\delta$, $\gamma$, $\Omega$, $\alpha$ and $n$ appear in our model and we have investigated the effect of $\Omega$, $\alpha$ and $n$ on the bifurcation diagrams for $\delta \ll 0$ and $\gamma \ll 0$. Although the results have been presented in this paper in a dimensionless form we noted earlier that the question of an appropriate scaling for the present problem is a difficult one. For this reason we will discuss the effect of model parameters on the bifurcation diagram in both dimensional and dimensionless forms. This will demonstrate our earlier claim that the key features of the bifurcation diagrams do not depend on the choice of characteristic scales for the problem.

The effect of particle-phase viscosity on the bifurcation diagram was examined by varying $A$ over 2 orders of magnitude. An analysis of the linear stability of the uniform state reveals that the dimensional vertical wavenumber at the Hopf bifurcation, $L_{HB}$, is proportional to $\{\mu_s(\phi_0)\}^{1/2}$ (or equivalently to $A^{1/2}$). Our choice of characteristic length scale captures this dependence. This is also true for the scaling adopted by

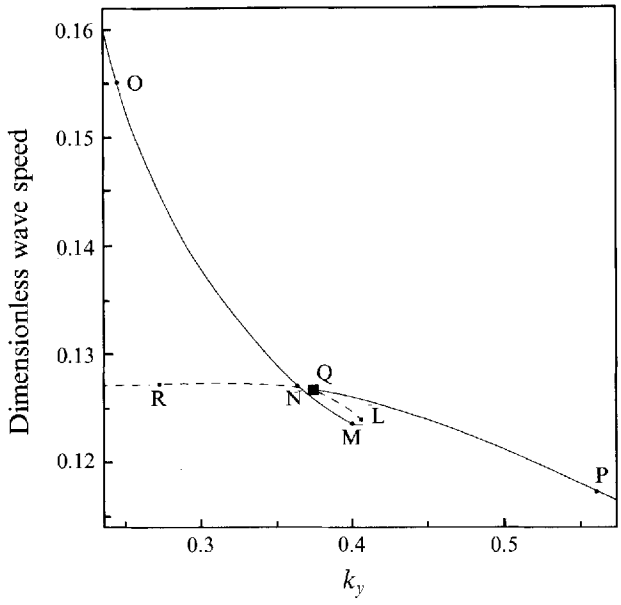


FIGURE 16. Dimensionless wave speed of one- and two-dimensional travelling waves. $\phi_0 = 0.57$. $k_x = k_y$. The labelled points correspond to their namesakes in figure 10. The solid curve indicates stable solutions. The broken curve indicates unstable solutions.

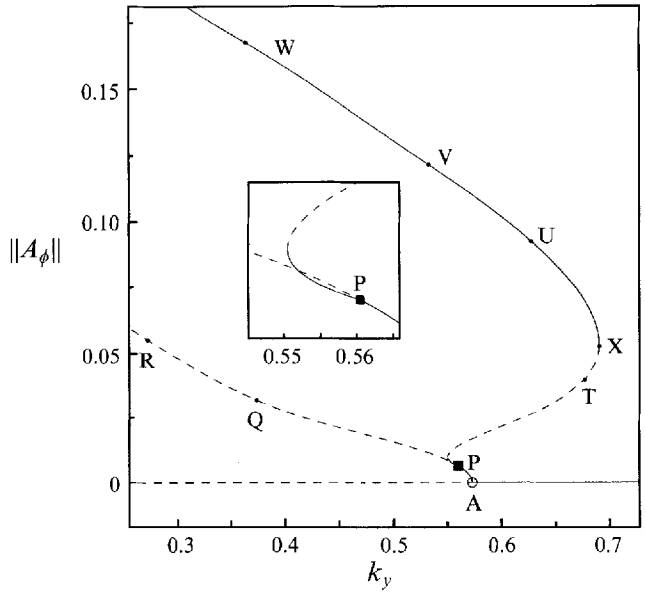


FIGURE 17. Bifurcation diagram for fixed lateral wavenumber, $k_x = 0.182$. $\phi_0 = 0.57$. Points P, Q and R on the 1D-TW branch correspond to their namesakes in figure 2.

Ganser & Drew (1990), who explicitly chose $L_{HB}$ as the characteristic length. Their approach, however, is only valid for $\phi_0 < \phi_c$ and the length scale depends on the value of $\phi_0$ adopted. We chose our length scale to be independent of $\phi_0$ as we wanted to investigate the solution structure for a range of $\phi_0$ values, including cases where $\phi_0 > \phi_c$ and the uniform state is linearly stable.

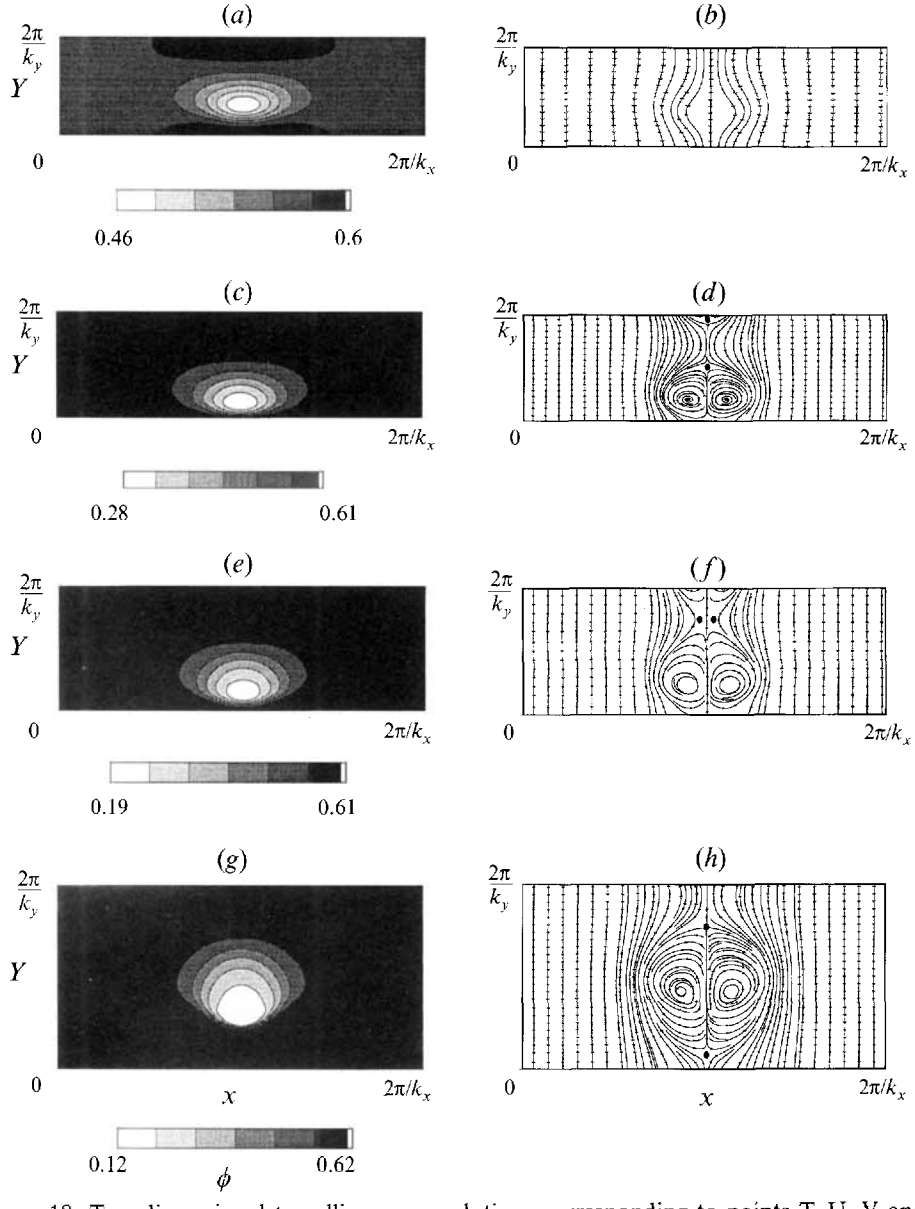


FIGURE 18. Two-dimensional travelling wave solutions corresponding to points T, U, V and W in figure 17. On the left are grey-scale plots of volume fraction of solids and on the right are the corresponding streamline plots of gas velocity. Stagnation points of saddle type are marked •. (*a*), (*b*) $k_y = 0.677, k_x = 0.182$, point T. $N = 9, M = 7$. (*c*), (*d*) $k_y = 0.628, k_x = 0.182$, point U. $N = 9, M = 7$. (*e*), (*f*) $k_y = 0.533, k_x = 0.182$, point V. $N = 10, M = 8$. (*g*), (*h*) $k_y = 0.364, k_x = 0.182$, point W. $N = 24, M = 16$.

In a dimensionless formulation varying the magnitude of the particle-phase viscosity is equivalent to changing $\Omega$, while holding all other parameters constant. (Although $\gamma$ depends on the magnitude of the particle-phase viscosity, this has a negligible effect because $\gamma \ll 1$). We found that the qualitative features of the bifurcation diagram were not affected for a change in $\Omega$ spanning an order of magnitude.

We have also examined the effect of setting $\mu_s$ to a constant value (independent

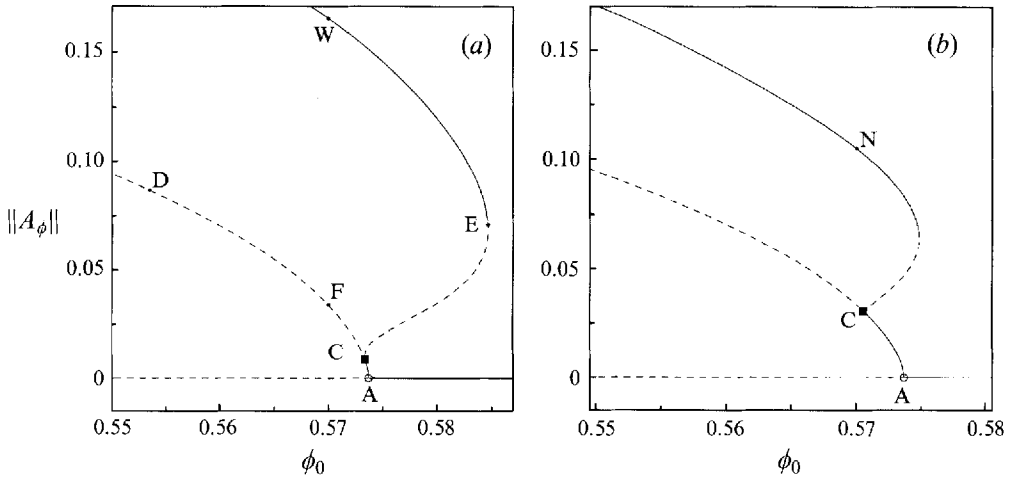


FIGURE 19. Bifurcation diagrams with $\phi_0$ as the parameter. (*a*) $k_x = 0.364, k_y = 0.182$. Point W corresponds to its namesake in figure 17. (*b*) $k_x = k_y = 0.364$. Point N corresponds to its namesake in figure 10.

of $\phi$), namely $\mu_s = 13.3A = 6.65$ P, which can be obtained by setting $\phi = \phi_0 = 0.57$ in (10) with $A = 0.5$ P. The bifurcation diagram shown in figure 20 (for constant $\mu_s$) corresponds to the conditions of figure 10 (for $\phi$-dependent $\mu_s$). These two bifurcation diagrams are qualitatively similar. On the 2D-TW branch (CEF in figure 20), we initially see the same development of lateral structure as seen earlier in figure 10. Figure 21(*a*) corresponding to a point on the 2D-TW branch next to point C in figure 20 is similar to figure 11(*a*) described earlier. The $\phi$-structure at point E in figure 20 is shown in figure 21(*b*). The voidage hole in this case has a semi-circular shape, which differs from those shown in figures 12(*a*), 13(*a*) and 14(*a*). Figure 22 presents the solution corresponding to point F in figure 20. Some concavity has developed in the floor of the voidage hole and the shape of this hole has a strong resemblance to bubbles observed in fluidized beds. The circulation pattern in the gas (figure 22*b*) is displaced forward relative to the centre of the voidage hole. These results are encouraging, as it is now clear that small changes in the closure relations can produce realistic shapes for voidage holes.

The effect of particle pressure has also been investigated by changing both the magnitude of $p_s$ and the closures adopted. For the closure in (8) we have considered different values of $C_1$ spanning an order of magnitude. Increasing $C_1$ (which is equivalent to increasing the dimensionless particle pressure coefficient, $\alpha$, while holding all other dimensionless groups constant) increases $\phi_c$ and thus 'shifts' the bifurcation diagram in $\phi_0$. This can be illustrated by expressing the structure of the 1D-TWS shown in figure 2 in a more general form as follows. When $\phi_0$ is slightly less than $\phi_c$, the 1D-TWs emerge from the uniform state through a subcritical Hopf bifurcation. As $\phi_c - \phi_0$ increases, this changes to a supercritical bifurcation. When $\phi_0 = \phi_c$, the Hopf bifurcation point coincides with the origin. For $\phi_0$ slightly larger than $\phi_c$, the 1D-TWs exist as an isolated branch. The 2D-TWs in turn bifurcate from the 1D-TWs as discussed in §6.

In order to investigate the sensitivity of the results to changes in the closure for $p_s$, we repeated our calculations using the closure relation in (9) with $(m_1 = 1, m_2 = 0)$ and $(m_1 = 1, m_2 = 2)$. In both cases, the value of the coefficient $C_2$ was so chosen

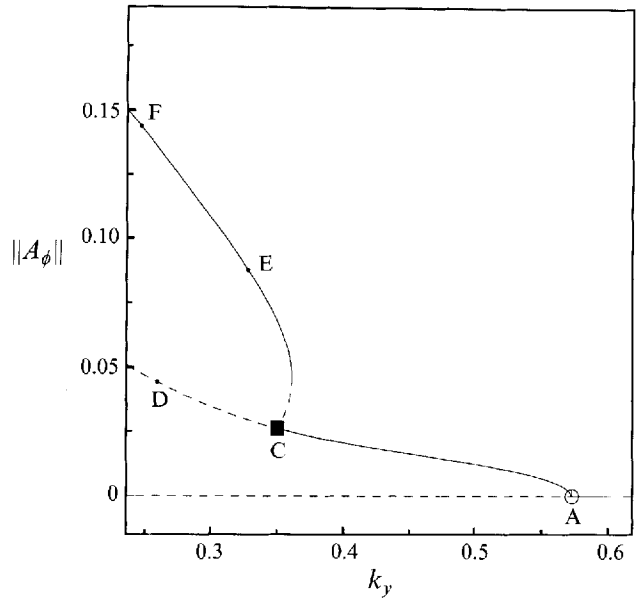


FIGURE 20. Bifurcation diagram for constant solids viscosity. $\mu_s = 13.3A = 6.65$ P = constant, independent of $\phi$. $\phi_0 = 0.57$. $k_x = k_y$. Model parameters and dimensionless groups are presented in table 1.

that $p_s$ computed from (9) at $\phi = \phi_0 = 0.57$ was the same as that given by (8). The value of the solids viscosity was kept constant at $\mu_s = 13.3A = 6.65$ P. The bifurcation diagrams computed with these two cases are illustrated in figure 23. In both cases, 1D-TWs emerge from the uniform state and 2D-TWs bifurcate from the 1D-TWs. The first case ($m_1 = 1, m_2 = 0$) describes a linear variation of $p_s$ with $\phi$ and for the chosen parameters the 2D-TW branch bifurcates supercritically from the 1D-TW branch. Furthermore the high-amplitude 1D-TWs solutions do not develop the strongly asymmetric $\phi$-profiles discussed earlier, but instead remain fairly sinusoidal. This lack of asymmetry can also be observed in the high-amplitude 2D-TWs where the voidage hole does not become localized in space. The bifurcation diagram for the second case ($m_1 = 1, m_2 = 2$) has features that are similar to those described earlier with $p_s$-closure given by (8) (see figure 20).

In order to ascertain the effect of the Richardson–Zaki exponent on the bifurcation diagram, we performed calculations corresponding to the conditions of figure 10 with a different Richardson–Zaki exponent, namely $n = 3.35$. We found that the qualitative features of the bifurcation diagram remained unchanged. We have also investigated the effect of particle diameter on the bifurcation behaviour. It is known from experiments that bubbling occurs over a wide range of particle sizes so it is important to perform calculations for various particle sizes to confirm the generality of the results we have obtained. Increasing the particle size leads to an increase in the particle terminal velocity, $v_t$, and a decrease in the Richardson–Zaki exponent, $n$, and thus a decrease in $\beta$. In practice the particle size may also affect the effective mechanical properties of the particulate phase, namely the particle-phase pressure and viscosity. However, as discussed by Batchelor (1988) our understanding of the mechanics of suspensions is not yet adequate to link the effective properties of the suspension to the physical properties of the fluid and the particles.

We computed bifurcation diagrams for a range of particle diameters (200 –

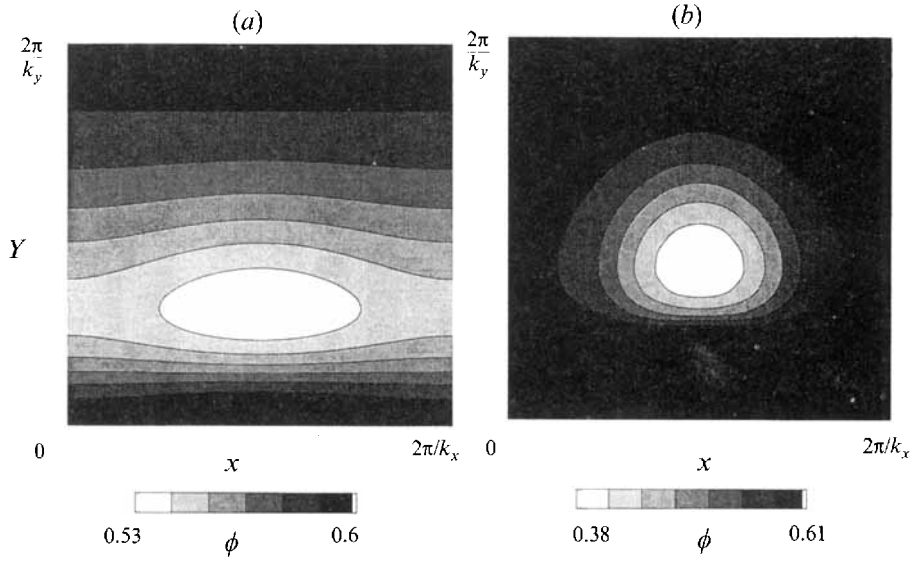


FIGURE 21. Two-dimensional travelling wave solutions corresponding to points C and E in figure 20. Grey-scale plots of volume fraction of solids for: (*a*) solution near (indistinguishable from) point C in figure 20. $k_y = k_x = 0.351$. $N = 9, M = 7$. (*b*) Solution corresponding to point E in figure 20. $k_y = k_x = 0.328$. $N = 18, M = 13$.

$-1000\,\mu$m) taking into consideration the effect of particle size on only $v_t$ and $n$. In terms of dimensionless groups this is equivalent to varying $\Omega$, $\alpha$ and $n$ simultaneously. The bifurcation diagrams have been computed for $\phi_0$ slightly less than $\phi_c$ where the value of $\phi_c$ decreases with an increase in particle size. Figure 24 shows the volume fraction norm, $\|A_\phi\|$, as a function of $k_y$ for a bed for $300\,\mu$m diameter glass beads fluidized by air. (Model parameters are shown in the second column of table 1.) This figure showing the uniform state, 1D-TW and 2D-TW, illustrates the robustness of the bifurcation behaviour.

## 8. Discussion

We have established that the existence of bubble-like solutions for gas-fluidized beds is a robust phenomenon, independent of the specific closures used to describe the particle-phase pressure and viscosity. The common features obtained with every closure scheme analysed are the birth of 1D-TWs from the uniform state and the emergence of 2D-TWs from the 1D-TWs. It is also seen that high-amplitude travelling wave solutions can coexist with stable uniform states.

Bubble development has been visualized by Batchelor (1991) as a sequence of four stages: a 1D-TW evolves from an unstable uniform state in the first stage, and this wave develops a two-dimensional structure through an overturning instability in the second stage; particles are expelled from a region with smaller-than-average particle concentration in the third stage and a steadily rising bubble of clear fluid with a steady shape develops in the final stage.

As the fastest growing instability away from the unstable uniform state is a 1D-TW, it is indeed reasonable to expect the bubbles to evolve initially as 1D-TWs and subsequently develop two-dimensional structure. In all probability the evolution of two-dimensional structure will start before the 1D-TW becomes fully developed.

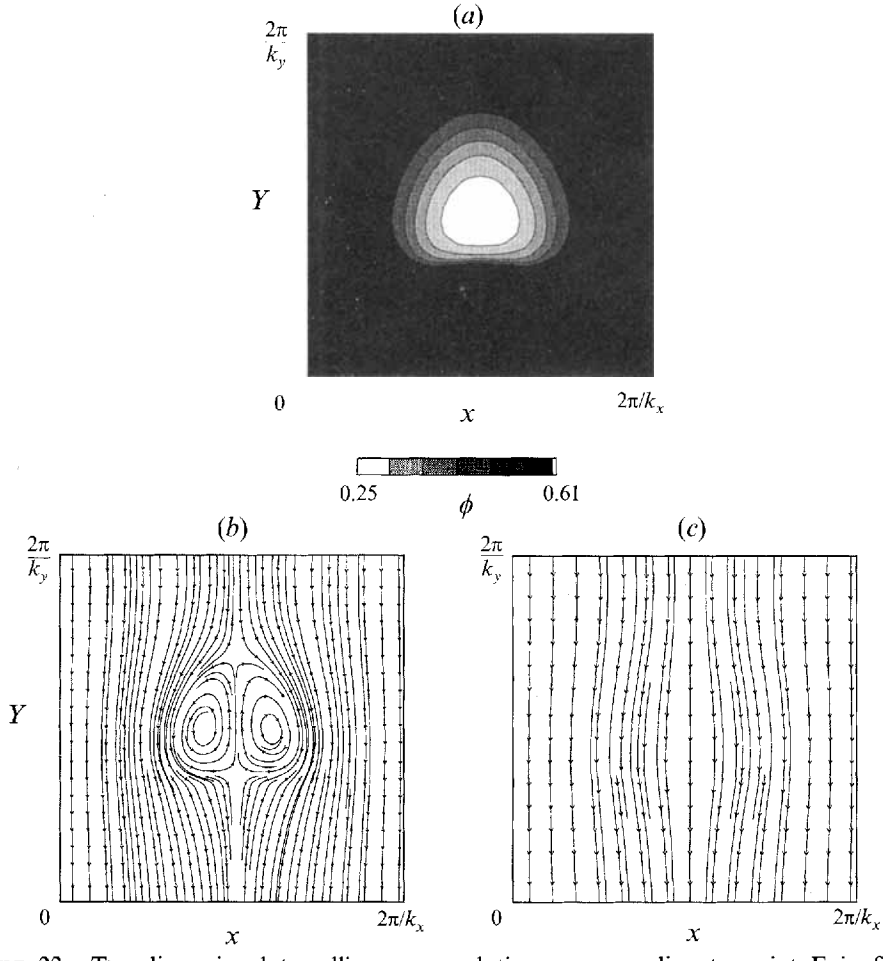


FIGURE 22. Two-dimensional travelling wave solution corresponding to point F in figure 20. $k_y = k_x = 0.248$. $N = 27, M = 18$. (*a*) Volume fraction of solids. (*b*) Streamline plot of gas velocity. (*c*) Streamline plot of solids velocity.

However, as the growth rates of 1D-TW from the uniform state and the 2D-TW from a fully developed 1D-TW are of comparable magnitude, it seems reasonable to seek the mechanism behind the second stage of bubble development by examining the instability of the *fully developed* 1D-TWs to two-dimensional perturbations.

Consider the four fully developed 1D-TWs shown in figure 3. The growth rates of two-dimensional perturbations of each of these 1D-TWs is presented in figure 4, as a function of the transverse wavenumber, $k_x$. The eigenfunctions corresponding to the most unstable eigenvalue of each of these four waves are shown in figures 5 to 8. An examination of these eigenfunctions reveals several features:

(i) In every case, the instability of the 1D-TWs takes the form of alternating columns of upward and downward moving fluid and solid, which change direction every half-wavelength in the lateral direction.

(ii) In every upward moving column, the region with the highest voidage coincides with the region with the highest velocity of upward moving fluid, while the region with the highest particle concentration has the highest velocity of upward moving solids. In the downward moving columns, the opposite picture holds.

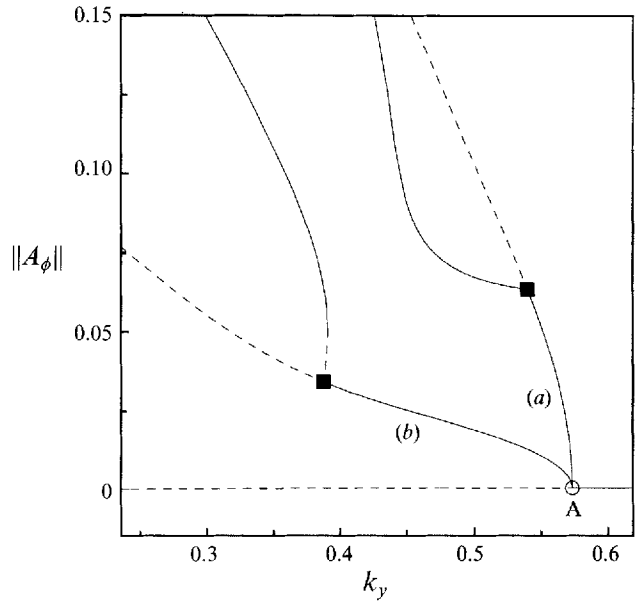


FIGURE 23. Bifurcation diagram with $p_s$-closure given by equation (9). $\phi_0 = 0.57$. $k_y = k_x$. $\mu_s = 13.3A = 6.65$ P = constant, independent of $\phi$. (*a*) $m_1 = 1, m_2 = 0$. (*b*) $m_1 = 1, m_2 = 2$.

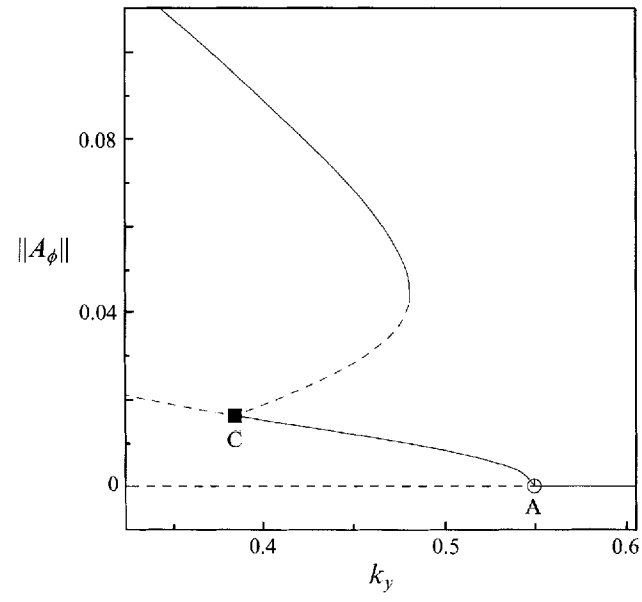


FIGURE 24. Bifurcation diagram for 300 μm diameter glass beads. $\phi_0 = 0.586$. $k_x = 0.185$.

(iii) As the amplitude of the 1D-TW increases, the eigenfunctions for the fluid and solid velocities manifest progressively larger lateral movement between the upward and downward moving columns. This is accompanied by a decrease in the aspect ratio of the cell ($= k_y/k_x$) for which the growth rate of the two-dimensional perturbations is largest.

The extent of lateral movement of fluid and solid between the upward and downward moving columns is related to the aspect ratio of the cell. Very little lateral

movement of fluid and solids is seen in figures 5(*c*) and 5(*d*) simply because of the fact that $k_x \ll k_y$. If we examine a case where $k_x \approx k_y$ we see a greater lateral migration even for a low-amplitude wave. In a similar fashion, the two-dimensional velocity eigenfunctions for the high-amplitude wave in figure 8(*a*) corresponding to a cell with $k_x \ll k_y$ do not have a large amount of lateral movement (not shown). Thus we can conclude that the amplitude of the 1D-TW determines the aspect ratio of the most unstable two-dimensional disturbance, which in turn controls the extent of lateral movement of fluid and solid seen in the eigenfunctions.

We traced the origin of these eigenfunctions back to the uniform state by examining the stability of a family of 1D-TWs obtained by varying $k_y$ while holding $k_x$ fixed. We present the case where we start at conditions corresponding to the positive real eigenvalue at point g ($k_y = 0.373$, $k_x = 0.138$) in figure 4; see figure 7 for the corresponding eigenfunction. As $k_y$ is increased while $k_x$ is held constant at 0.138 the amplitude of the corresponding 1D-TW decreases and the real eigenvalue in question decreases in magnitude and approaches zero. The eigenvalue passes through zero at $k_y = 0.569$ and the corresponding eigenfunctions for the solids fraction and fluid velocity in the wave frame are shown in figures 25(*a*) and 25(*b*) respectively. The solids velocity is not shown but is similar to the fluid velocity. As $k_y$ is increased further the 1D-TW continues to decrease in amplitude and the eigenvalue recedes in the negative half-plane, and remains real. At $k_y = 0.573$ we have a very small-amplitude 1D-TW and the corresponding eigenfunctions for the solids fraction and fluid velocity are shown in figures 25(*c*) and 25(*d*) respectively.

At $k_y = 0.5735$ the amplitude of the 1D-TW becomes zero and we are left with examining the stability of the uniform state. At the uniform state the eigenvalue in question is still real and the corresponding eigenfunctions of solids fraction and fluid velocity are plotted in figures 25(*e*) and 25(*f*) respectively. It was found that the real eigenvalue at the uniform state is independent of $k_y$ and the eigenfunction only has structure in the $x$-direction so that it corresponds to a transverse-only mode. This mode takes the form of alternating columns of upward and downward moving fluid and particles.

An examination of the other three 1D-TWs shown in figure 3 and the corresponding eigenfunctions in figures 5, 6 and 8 reveals a similar picture involving the interaction between the 1D-TW and transverse-only mode, i.e. it is the descendant of the transverse-only mode of the uniform state which interacts with the 1D-TW and leads to the instability of the 1D-TW.

We also examined the origin of the eigenfunction corresponding to the instability of the 1D-TW for the case where $\mu_s$ is a constant value (independent of $\phi$) and $p_s$ varies linearly with $\phi$. The model parameters are as in figure 23 (see §7). We examined the stability of a family of 1D-TWs obtained by varying $k_y$ while holding $k_x$ fixed at 0.138. The trend described above is still seen and as $k_y$ is increased while $k_x$ is held constant the amplitude of the corresponding 1D-TW decreases and the real eigenvalue in question decreases in magnitude and approaches zero. The eigenvalue passes through zero at $k_y = 0.5733$ and the corresponding eigenfunctions for the solids fraction and fluid velocity in the wave frame are shown in figures 26(*a*) and 26(*b*), which are very similar to figures 25(*a*) and 25(*b*). As $k_y$ is increased further the 1D-TW continues to decrease in amplitude and the eigenvalue recedes in the negative half-plane and 'collides' with another real eigenvalue to become a pair of complex-conjugate eigenvalues.

At $k_y = 0.5734$ we again have a very small-amplitude 1D-TW and in figures 26(*c*) and 26(*d*) we plot the solids fraction and fluid velocity eigenfunctions corresponding to

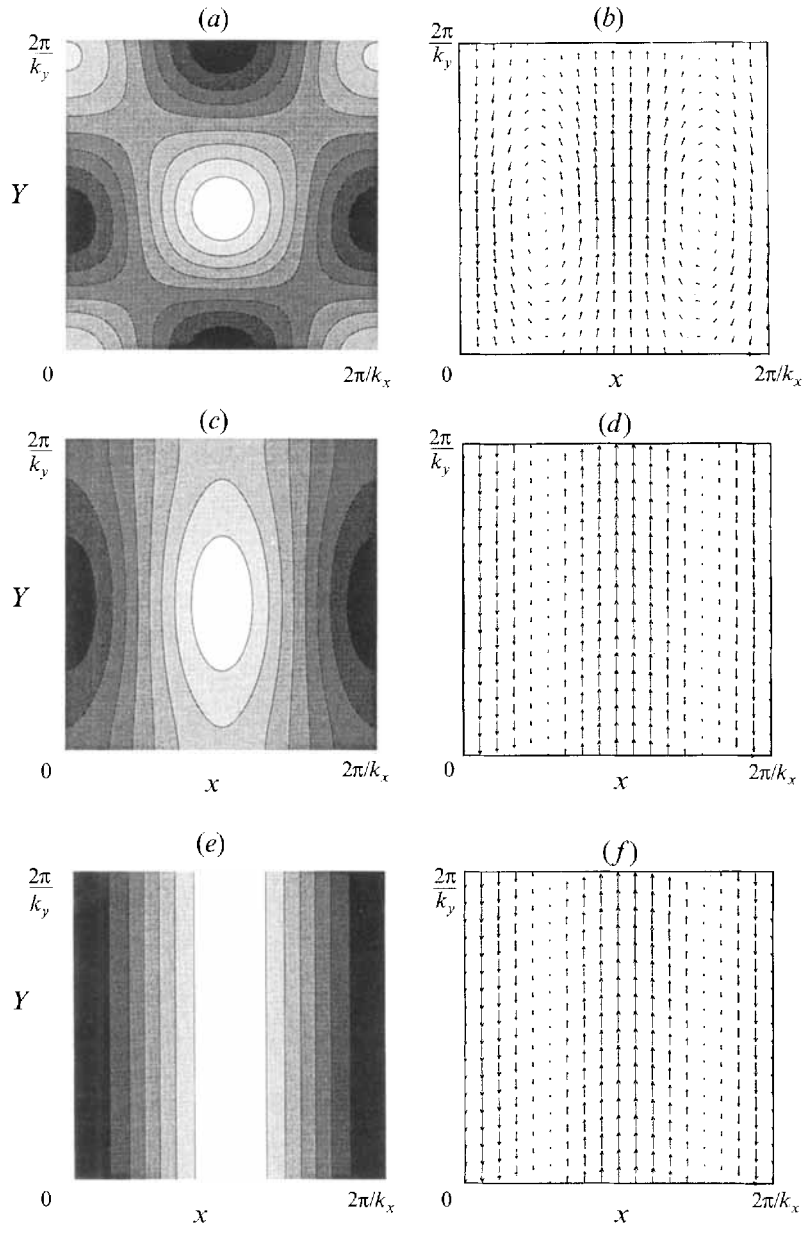


FIGURE 25. Continuation of the critical eigenfunction, corresponding to instability of the 1D-TW, back to the uniform state. On the left are grey-scale plots of the $\phi$-eigenfunctions and on the right are vector plots of gas-velocity eigenfunctions. (*a*), (*b*) 1D-TW with $k_y = 0.569, k_x = 0.138$. (*c*), (*d*) 1D-TW with $k_y = 0.573, k_x = 0.138$. (*e*), (*f*) Uniform state with $k_y = 0.5735, k_x = 0.138$. Eigenfunctions are shown in a square box to facilitate comparison.

the complex-conjugate pair of eigenvalues in question. At $k_y = 0.5735$ the amplitude of the 1D-TW becomes zero and the solids fraction and fluid velocity eigenfunctions of the complex-conjugate pair now at the uniform state are plotted in 26(*e*) and 26(*f*). The complex-conjugate pair of eigenvalues has structure in both the $x$- and $y$-directions and corresponds to a mixed mode. This mode takes the form of a

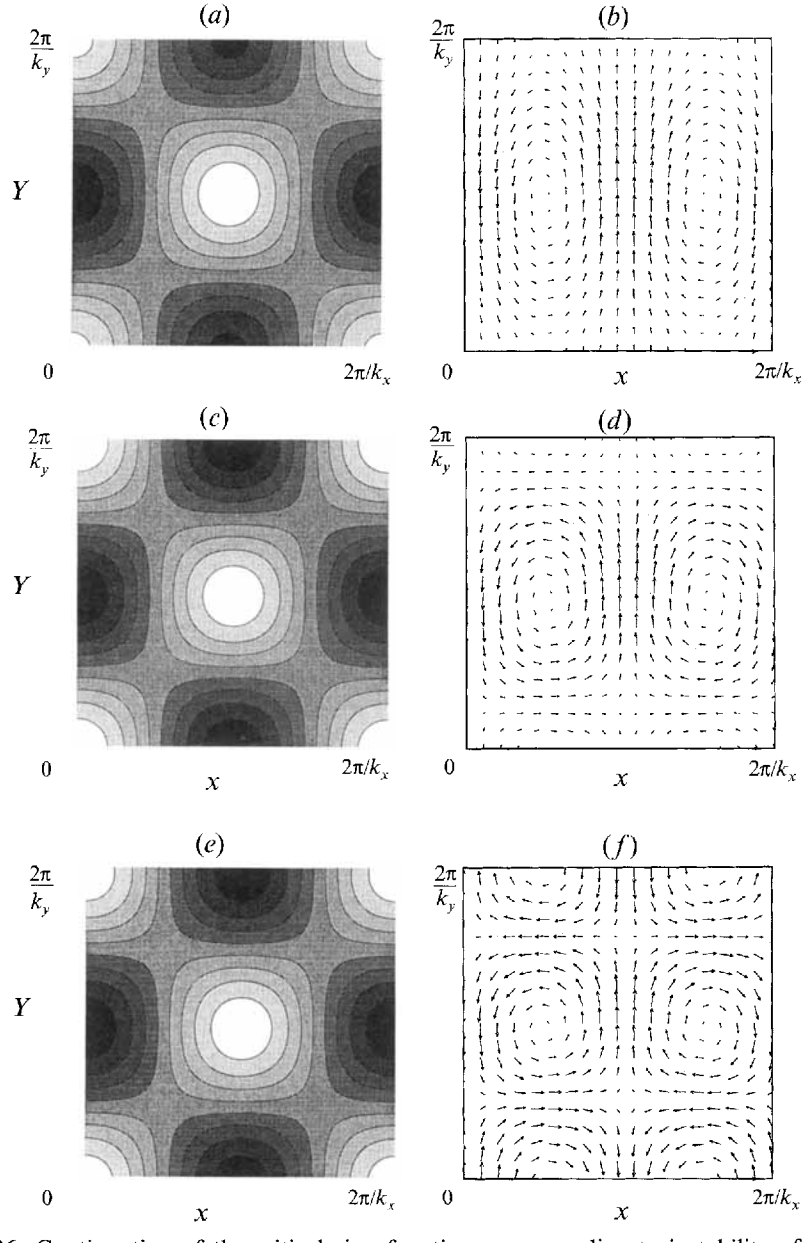


FIGURE 26. Continuation of the critical eigenfunction corresponding to instability of the 1D-TW back to the uniform state for $p_s$-closure given by equation (9) with $m_1 = 1, m_2 = 0$. On the left are grey-scale plots of the $\phi$-eigenfunctions and on the right are vector plots of gas-velocity eigenfunctions. (*a*), (*b*) 1D-TW with $k_y = 0.5733, k_x = 0.138$. (*c*), (*d*) 1D-TW with $k_y = 0.5734, k_x = 0.138$. (*e*), (*f*) Uniform state with $k_y = 0.5735, k_x = 0.138$.

recirculation in the fluid velocity with a large amount of lateral movement of fluid; this lateral movement of material is also seen in the solids velocity (not shown).

This latter case was examined by Göz (1995*b*) and he also found that it was the descendant of the mixed mode of the uniform state that interacts with the 1D-TW and leads to the instability of the 1D-TW. Therefore the different closures lead to a different origin of the eigenfunction responsible for the instability; this is explained in

detail by Göz (1995*b*). However, for all the cases we have examined we have observed that at or beyond the critical conditions (where the real eigenvalue passes through zero and moves into the positive half-plane) the corresponding eigenfunctions always have the same basic features described above (for figures 5, 6, 7 and 8).

Batchelor & Nitsche (1991) have analysed the stability of a fluid, whose density is sinusoidally modulated in the vertical direction, to two-dimensional perturbations. It was assumed the density variation resulted from a variation in the concentration of some material in the fluid, and equations describing the evolution of the disturbance were formulated in terms of an average velocity and concentration of the diffusing material. The eigenfunctions corresponding to the most unstable eigenvalue that they obtained are strikingly similar to those observed in the present study, the most notable feature being the alternating columns of upward and downward moving material. This leads us to conclude that the mechanism through which two-dimensional structure evolves in our problem is analogous to the overturning instability discussed by Batchelor & Nitsche (1991).

In order to fully understand the differences between bubbling and non-bubbling systems, a bifurcation analysis of the type described here should be carried out for $\delta$-values corresponding to liquid-fluidized beds. However, no fully developed, constant-shape two-dimensional structures were observed by Anderson *et al.* (1995) in their numerical simulation of liquid-fluidized beds. This suggests that the solution structure of liquid-fluidized beds may not be completely captured by continuation and stability analysis of constant-shape travelling waves of the type analysed here; these should be complemented by extensive transient integrations of the ensemble-averaged equations to locate both spatially and temporally oscillating waves. We are in the process of developing these computational tools.

This work has been partially supported by the National Science Foundation, the Mobil Foundation, the Exxon Education Foundation and ARPA/ONR. The computational work was carried out through a grant of time on a CRAY C90 from the Pittsburgh Supercomputing Center. We would like to acknowledge the considerable help and advice we received from Roy Jackson, Karl Anderson and Manfred Göz over the course of this work.

## REFERENCES

ANDERSON, K., SUNDARESAN, S. & JACKSON, R. 1995 Instabilities and the formation of bubbles in fluidized beds. *J. Fluid Mech.* **303**, 327–366.

ANDERSON, T. B. & JACKSON, R. 1967 Fluid mechanical description of fluidized beds. Equations of motion. *Indust. Engng Chem. Fundam.* **6**, 527–539.

ANDERSON, T. B. & JACKSON, R. 1968 Fluid mechanical description of fluidized beds. Stability of the state of uniform fluidization. *Indust. Engng Chem. Fundam.* **7**, 12–21.

ANDERSON, T. B. & JACKSON, R. 1969 Fluid mechanical description of fluidized beds. Comparison of theory and experiment. *Indust. Engng Chem. Fundam.* **8**, 137–144.

BATCHELOR, G. K. 1988 A new theory of the instability of a uniform fluidized bed. *J. Fluid Mech.* **193**, 75–110.

BATCHELOR, G. K. 1991 The formation of bubbles in fluidized beds. In *Proc. Honoring John W. Miles on his 70th birthday*. Scripps Institution of Oceanography, Ref. Series, pp. 91–24.

BATCHELOR, G. K. 1993 Secondary instability of a gas fluidized bed. *J. Fluid Mech.* **257**, 359–371.

BATCHELOR, G. K. & NITSCHE, J. M. 1991 Instability of stationary unbounded stratified fluid. *J. Fluid Mech.* **227**, 357–391.

BERRYMAN, J. G. 1982 Random close packing of hard spheres and disks. *Phys. Rev.* A **27**, 1053–1062.

BOUILLARD, J. X. & GIDASPOW, D. 1991 On the origin of bubbles and Geldart's classification. *Powder Technol.* **68**, 13–22.

BROWN, H. S. & KEVREKIDIS, I. G. 1995 Modulated traveling waves for the Kuramoto-Sivashinsky equation. In *Fields Inst. Commun., Vol. 5: Applications of Pattern Formation and Symmetry Breaking in PDEs.* AMS (to appear).

BUYEVICH, Y. A. 1972 Statistical hydromechanics of disperse systems. Part 3. Pseudo-turbulent structure of homogeneous suspensions. *J. Fluid Mech.* **56**, 313–336.

CANUTO, C., HUSSAINI, M. Y., QUARTERONI, A. & ZANG, T. A. 1988 *Spectral Methods in Fluid Dynamics.* Springer.

CLIFT, R., GRACE, J. R., CHEUNG, L. & DO, T. H. 1972 Gas and solids motion around deformed and interacting bubbles in fluidized beds. *J. Fluid Mech.* **51**, 187–205.

DANKWORTH, D. C. & SUNDARESAN, S. 1991 Time-dependent flow patterns arising from the instability of uniform fluidization. Presentation at *Symposium on the Mechanics of Fluidized Beds* , Stanford University.

DIDWANIA, A. K. & HOMSY, G. M. 1981 Flow regimes and flow transitions in liquid fluidized beds. *Intl J. Multiphase Flow* **7**, 563–580.

DIDWANIA, A. K. & HOMSY, G. M. 1982 Resonant side-band instabilities in wave propagation in fluidized beds. *J. Fluid Mech.* **122**, 433–438.

DOEDEL, E., KELLER, H. & KERNEVEZ, J. 1991 Numerical analysis and control of bifurcation problems. I: Bifurcation in finite dimensions. *Intl J. Bifurcation Chaos* **1**, 493–520.

DREW, D. A. 1971 Averaged field equations for two-phase media. *Stud. Appl. Maths* **50**, 133–166.

DREW, D. A. & SEGEL, L. A. 1971 Averaged equations for two-phase flows. *Stud. Appl. Maths* **50**, 205–231.

EL-KAISSY, M. M. & HOMSY, G. M. 1976 Instability waves and the origin of bubbles in fluidized beds. I: Experiments. *Intl J. Multiphase Flow* **2**, 379–395.

ERGUN, S. 1952 Fluid flow through packed columns. *Chem. Engng Prog.* **48**, 89–94.

FANUCCI, J. B., NESS, N. & YEN, R.-H. 1979 On the formation of bubbles in gas-particulate fluidized beds. *J. Fluid Mech.* **94**, 353–367.

FANUCCI, J. B., NESS, N. & YEN, R.-H. 1981 Structure of shock waves in gas-particulate fluidized beds. *Phys. Fluids* **24**, 1944–1954.

FOSCOLO, P. U. & GIBILARO, L. G. 1984 A fully predictive criterion for the transition between particulate and aggregative fluidization. *Chem. Engng Sci.* **39**, 1667–1675.

FOSCOLO, P. U. & GIBILARO, L. G. 1987 Fluid dynamic stability of fluidized suspensions: the particle bed model. *Chem. Engng Sci.* **42**, 1489–1500.

GANSER, G. H. & DREW, D. A. 1990 Nonlinear stability analysis of a uniform fluidized bed. *Intl J. Multiphase Flow* **16**, 447–460.

GARG, S. K. & PRITCHETT, J. W. 1975 Dynamics of gas fluidized beds. *J. Appl. Phys.* **46**, 4493–4500.

GIDASPOW, D., SYAMLAL, M. & SEO, Y. C. 1986 Hydrodynamics of fluidization: supercomputer generated vs. experimental bubbles. *J. Powder Bulk Solids Tech.* **10**, 19–23.

GLASSER, B. J. 1995 The development of bubbles in fluidized beds. PhD dissertation, Princeton University.

GÖZ, M. F. 1992 On the origin of wave patterns in fluidized beds. *J. Fluid Mech.* **240**, 379–404.

GÖZ , M. F. 1993*a* Bifurcation of plane voidage waves in fluidized beds. *Physica* D **65**, 319–351.

GÖZ, M. F. 1993*b* Instabilities and the formation of wave patterns in fluidized beds. In *Instabilities in Multiphase Flows* (ed. G. Gouesbet & A. Berlemont), pp. 251–259. Plenum.

GÖZ, M. F. 1995*a* Secondary instability in gas-fluidized beds. *Z. Angew. Math. Mech.* **75**, SI, S381–S382.

GÖZ, M. F. 1995*b* Transverse instability of plane wavetrains in gas-fluidized beds. *J. Fluid Mech.* **303**, 55–82.

HERNÁNDEZ, J. A. & JIMÉNEZ, J. 1991 Bubble formation in dense fluidized beds. In *Proc. NATO Advanced Research Workshop on the Global Geometry of Turbulence* (ed. J. Jiménez), pp. 133–142. Plenum.

HINCH, E. J. 1977 An averaged-equation approach to particle interactions in a fluid suspension. *J. Fluid Mech.* **83**, 695–720.

HOMSY, G. M., EL-KAISSY, M. M. & DIDWANIA, A. 1980 Instability waves and the origin of bubbles in fluidized beds. II: Comparison with theory. *Intl J. Multiphase Flow* **6**, 305–318.

JACKSON, R. 1963*a* The mechanics of fluidized beds. I: The stability of the state of uniform fluidization. *Trans. Inst. Chem. Engrs* **41**, 13–21.

JACKSON, R. 1963*b* The mechanics of fluidized beds. II: The motion of fully developed bubbles. *Trans. Inst. Chem. Engrs* **41**, 22–28.

JOHNSON, P. C. & JACKSON, R. 1987 Frictional-collisional constitutive relations for granular materials, with application to plane shearing. *J. Fluid Mech.* **176**, 67–93.

JOSEPH, D. D. & LUNDGREN, T. S. 1990 Ensemble average and mixture theory equations for incompressible fluid-particle suspensions. *Intl J. Multiphase Flow* **16**, 35–42.

KOCH, D. L. 1990 Kinetic theory for a monodisperse gas-solid suspension. *Phys. Fluids* A **2**, 1711–1723.

KUIPERS, J. A. M., PRINS, W. & VAN SWAAIJ, W. P. M. 1991 Theoretical and experimental bubble formation at a single orifice in a two-dimensional gas-fluidized bed. *Chem. Engng Sci.* **46**, 2881–2894.

KUNII, D. & LEVENSPIEL, O. 1991 *Fluidization Engineering*. Butterworth-Heinemann.

LIU, J. T. C. 1982 Note on a wave-hierarchy interpretation of fluidized bed instabilities. *Proc. R. Soc. Lond.* A **380**, 229–239.

LIU, J. T. C. 1983 Nonlinear unstable wave disturbances in fluidized beds. *Proc. R. Soc. Lond.* A **389**, 331–347.

LOCKETT, M. J. & HARRISON, D. 1967 The distribution of voidage fraction near bubbles rising in gas fluidized beds. In *Proc. Intl Symp. on Fluidization* (ed. A. A. H. Drinkenburg), pp. 257–267. Netherlands University Press.

MURRAY, J. D. 1965 On the mathematics of fluidization. Part 1. Fundamental equations and wave propagation. *J. Fluid Mech.* **21**, 465–493.

MUTSERS, S. M. P. & RIETEMA, K. 1977 The effect of interparticle forces on the expansion of a homogeneous gas-fluidized bed. *Powder Technol.* **18**, 239–248.

NEEDHAM, D. J. & MERKIN, J. H. 1983 The propagation of a voidage disturbance in a uniform fluidized bed. *J. Fluid Mech.* **131**, 427–454.

NEEDHAM, D. J. & MERKIN, J. H. 1984 The evolution of a two-dimensional small-amplitude voidage disturbance in a uniformly fluidized bed. *J. Engng Maths* **18**, 119–132.

NEEDHAM, D. J. & MERKIN, J. H. 1986 The existence and stability of quasi-steady periodic voidage waves in a fluidized bed. *Math. Phys. Z. Angew.* **37**, 322–339.

NGUYEN, X. T., LEUNG, L. S. & WEILAND, R. H. 1973 On void fractions around a bubble in a two-dimensional fluidized bed. In *Proc. Intl Congress on Fluidization and its Applications* (ed. H. Angelino), pp. 230–239. Societé de Chimie Industrielle.

NIGMATULIN, R. I. 1979 Spatial averaging in the mechanics of heterogeneous and dispersed systems. *Intl J. Multiphase Flow* **5**, 353–385.

PIGFORD, R. L. & BARON, T. 1965 Hydrodynamic stability of a fluidized bed. *Indust. Engng Chem. Fundam.* **4**, 81–87.

PRITCHETT, J. W., BLAKE, T. R. & GARG, S. K. 1978 A numerical model of gas fluidized beds. *AICHE Symp. Ser. No. 176.* **74**, 134–148.

RICHARDSON, J. F. & ZAKI, W. N. 1954 Sedimentation and fluidization: Part I. *Trans. Inst. Chem. Engrs* **32**, 35–53.

RIETEMA, K. & PIEPERS, H. W. 1990 The effect of interparticle forces on the stability of gas-fluidized beds. I: Experimental evidence. *Chem. Engng Sci.* **45**, 1627–1639.

SYAMLAL, M. & O'BRIEN, T. J. 1989 Computer simulation of bubbles in a fluidized bed. *AIChE Symp. Ser. No. 270.* **85**, 22–31.

YATES, J. G., CHEESMAN, D. J. & SERGEEV, Y. A. 1994 Experimental observations of voidage distribution around bubbles in a fluidized bed. *Chem. Engng Sci.* **49**, 1885–1895.

ZHANG, D. Z. & PROSPERETTI, A. 1994 Averaged equations for inviscid disperse two-phase flow. *J. Fluid Mech.* **267**, 185–219.